HYDROMECHANICS

AERODYNAMICS

STRUCTURAL MECHANICS

APPLIED MATHEMATICS

ACOUSTICS AND VIBRATION

STEADY TWO-DIMENSIONAL PRESSURE DISTRIBUTIONS ON ARBITRARY PROFILES

by

Terry Brockett

HYDROMECHANICS LABORATORY

RESEARCH AND DEVELOPMENT REPORT

October 1965

Report 1821

STEADY TWO-DIMENSIONAL PRESSURE DISTRIBUTIONS ON ARBITRARY PROFILES

by

Terry Brockett

October 1965

Report 1821
S-R009-0101

TABLE OF CONTENTS

Page

LIST OF FIGURES

Page

LIST OF TABLES

PRINCIPAL NOTATION

A_n	Real part of complex transformation coefficient C_n
a	Radius of circle which is transformed to profile
a_n	Coefficient in Fourier series for ordinates
B_n	Multiple of i in the complex transformation coefficient C_n
b_n	Coefficient in Fourier series for ordinates
$C(\omega)$	Theoretical velocity on profile at zero angle of attack
C_c	Coefficient of force parallel to chord
$C_L = \frac{\text{Lift}}{1/2\rho U^2 c}$	Coefficient of force normal to direction of motion, "lift coefficient"
$C_m = \frac{\text{Moment}}{1/2\rho U^2 c^2}$	Moment coefficient, positive clockwise
C_N	Coefficient of force normal to the chordline
C_n	Complex transformation coefficient
$C_P = \frac{P - P_\infty}{1/2\rho U^2}$	Pressure coefficient
c	Chord length
$D(\varphi)$	Theoretical velocity on profile at $\alpha = 90°$
e	Base of natural logarithms
$F(\zeta)$	Complex potential in the plane of the circular cylinder
i	Imaginary constant, $i^2 = -1$
K	Modulus of complex transformation coefficient C_{-1}; equals 1/2 theoretical lift-slope coefficient
m, n	Index of summation
N	Number of angular intervals between 0 and π in numerical method (e.g., N = 18 in Figure 1)

P	Local static pressure
P_v	Vapor pressure of the liquid
P_∞	Pressure far from the profile
q	Magnitude of the velocity on the profile
R	Exponent of distortion variation
R_e	Reynolds numbers, based on chord length
$S(\omega)$	Combination of transformation coefficients
$T(\omega)$	Combination of transformation coefficients
t	Dummy integration variable
U	Asymptotic velocity in profile plane
V	Asymptotic velocity in circle plane
X_N	x-coordinate of profile nose
x	Abscissa in plane of profile
Y	Ordinate of profile
Y_C	Camberline ordinate
Y_{even}	Interpolation ordinate for $1/2\,(Y_U + Y_L)$, i.e., camber contribution
Y_L	Lower surface ordinate
Y_N	Ordinate of profile nose
Y_{odd}	Interpolation ordinate for $1/2\,(Y_U - Y_L)$, i.e., thickness contribution
Y_T	Thickness distribution ordinate
Y_U	Upper surface ordinate

z	Complex variable in plane of profile
α	Angle of incidence in plane of profile
α'	Empirical function to approximate boundary layer effects, chordwise variable
α_{o_e}	Experimental angle of zero lift
α_ζ	Angle of incidence in plane of circular cylinder
Γ	Circulation, lift/ρU
$\Delta\alpha$	Decrease in geometrical angle of attack to obtain actual lift
ζ	Complex variable in circle plane
n	Lift-slope coefficient, $(dC_L/d\alpha)_{\text{experiment}}/2\pi$
$\varkappa$	$\alpha - \alpha_\zeta$, equals theoretical angle of zero lift
λ	Index of summation
ν	Index of point at which velocity is obtained
ξ	Dummy integration variable
ρ	Fluid mass density
ρ_{LE}	Leading edge radius of curvature, nondimensional
$\sigma_i = \frac{P_\infty - P_v}{1/2\rho U^2}$	Cavitation index at inception or desinence of cavitation
τ	Thickness ratio, maximum distance from upper to lower surface of the thickness distribution divided by the chord
φ	Angular variable in circle plane, for the approximation it equals arc cos (2x - 1)
ω	Angle of rotation to put profile nose at (0,0)

ABSTRACT

A method of determining two-dimensional pressure distributions on arbitrary foils is explained. The development is based on an approximate potential theory suggested by Moriya (1941) which is empirically modified in a manner suggested by Pinkerton (1936) to give an arbitrary lift for a set incidence and at the same time satisfy the Kutta condition. Interpolation functions for the ordinates are used to reduce the calculations to a straightforward numerical procedure which is easily programmed for machine calculations. (FORTRAN statements for such a computer program are included.) The results are those of Riegels (1943).

Comparisons are made with other theoretical methods for potential flow and with experimental results. Good agreement with both calculated and measured pressure distributions is found when the lift coefficients are matched. The assumption that cavitation occurs when the local pressure falls to the vapor pressure is not upheld for the cases considered.

ADMINISTRATIVE INFORMATION

This report is essentially a duplication of a Master's Thesis submitted to the Graduate School of Cornell University in May 1965. The work was performed at the Taylor Model Basin under Bureau of Ships Subproject S-R009 01 01.

INTRODUCTION

To obtain an accurate estimate of the actual pressure distribution on two-dimensional forms, we have two approaches: (1) to solve the cumbersome Navier-Stokes equations governing viscous flow or (2) to use a potential theory with empirical modifications to approximate real fluid effects. The first approach may be simplified to solving the boundary-layer equations for a two-dimensional curved surface, but the simplification is nominal and the task remains formidable in application.[1,2] Moreover, as yet, this method is not sufficiently advanced to give accurate results unless experimental boundary-layer data are known.[3] The second possibility is based on potential theory which means simpler development and shorter computation time. As normally used, this method makes use of the experimental lift which is either available or can be estimated for conventional foils.

The first satisfactory method of using the experimental lift in potential theory was developed by Pinkerton in 1936.[4] He made use of the Betz (1915) observation[5] that employing the experimentally determined circulation in place of the theoretical value gives a pressure distribution that agrees well with measured results over most of the chord. However, merely inserting the experimentally determined circulation into potential theory will not, in general, satisfy the Kutta condition that the flow leave the trailing edge smoothly. Pinkerton[4] was able to retain the measured lift and also satisfy the smooth-flow condition by introducing an empirical modification in the profile shape. He applied the modification to a rigorous potential theory

[1] References are listed on page 72.

formulated by Theodorsen in 1932.[6] Although Theodorsen's theory is easier to apply than the boundary layer equations, the calculations are still lengthy.

Riegels[7] removed this last complication in 1943. He adopted Pinkerton's idea of an empirical distortion in the flow field to an approximate potential theory developed by Moriya in 1938.[8] Riegels made a further simplification by linearizing the equations on a small parameter introduced in the modification. In addition, he used interpolation functions for the ordinates which reduce the calculations to a straightforward numerical procedure, requiring only offsets at fixed fractions of the chord. The linearized numerical procedure of Riegels has been in use for some time* at the David Taylor Model Basin where it was programmed[9] for the computers at the Applied Mathematics Laboratory. In addition to giving the chordwise pressure distribution, the results of this program can be used to predict cavitation inception if the assumption is made that the cavitation starts when the local pressure falls to the vapor pressure of the surrounding liquid. Unfortunately, output from this program consists of the pressure distribution at only the input points so there is no assurance that the minimum is obtained. During the analysis necessary to correct this omission, it became obvious that the Riegels derivation was quite obscure. A detailed derivation of the theory was accordingly undertaken, and the results of the investigation are outlined in this paper. The derivation closely follows later work of Moriya[10] (1941) which is an approximate conformal transformation of the circle

*In 1955, a Model Basin Memorandum (Aero 28) described a method of calculating pressure distributions over profiles of arbitrary shapes. This memorandum included a translation of the Riegels paper (Reference 7).

to an airfoil profile and gives the same equations for the velocity distribution as his earlier work.

The present contribution to the development is a unified presentation of the theory, simplification and extension of the numerical method, and extensive comparisons with experiment and theory. In the comparisons with theory, some new results of considerable simplicity are derived from an exact conformal transformation of the circular cylinder (see Appendix A). Airfoil geometry is discussed in Appendix B.

The FORTRAN statements of a new computer program for calculating the pressure distribution on an arbitrary profile are given in the paper together with a description of the program and input instructions. The program statements are listed in Appendix C. This program will accept foil ordinates at arbitrary stations and interpolate between them to obtain the ordinates at the required stations.

POTENTIAL PRESSURE DISTRIBUTION FROM APPROXIMATE CONFORMAL MAPPING

SUMMARY OF DERIVATION

Using the method of conformal transformation, we can easily transform the known flow about a simple body to that about an arbitrary profile. As is customary, we take the circular cylinder for the simple body since both its geometry and complex potential are simple in form.

This development retains the two simplifying approximations made by Moriya[10]: (1) a group of transformation coefficients is ignored in the calculations and (2) the circulation is determined by placing a stagnation point at the trailing edge of this approximate transformation rather than the exact one. For symmetrical foils, the second approximation is exact.

COEFFICIENTS OF THE TRANSFORMATION

A difficulty with all transformations of the circle into an airfoil is that of matching the coefficients of the transformation with those of the airfoil. Except for special cases, iteration is required. In the work that follows, we neglect the iteration and instead evaluate the coefficients with a first approximation to the transformation.

The most general mapping function which maintains the type (but not necessarily magnitude and direction) of the flow at large distances from the body is given by

$$z = C_{-1}\frac{\zeta}{a} + C_o + \sum_1^\infty C_n \frac{a^n}{\zeta^n} = x + iy \qquad [1]$$

where z is the complex coordinate in the profile plane,

$C_n = A_n + i B_n$,

$n = -1, 0, 1, 2, \ldots$

ζ is the complex variable in the circle plane, and

$\zeta = re^{i\omega}$, as shown in the figure below which also shows the orientation of the flow velocity.

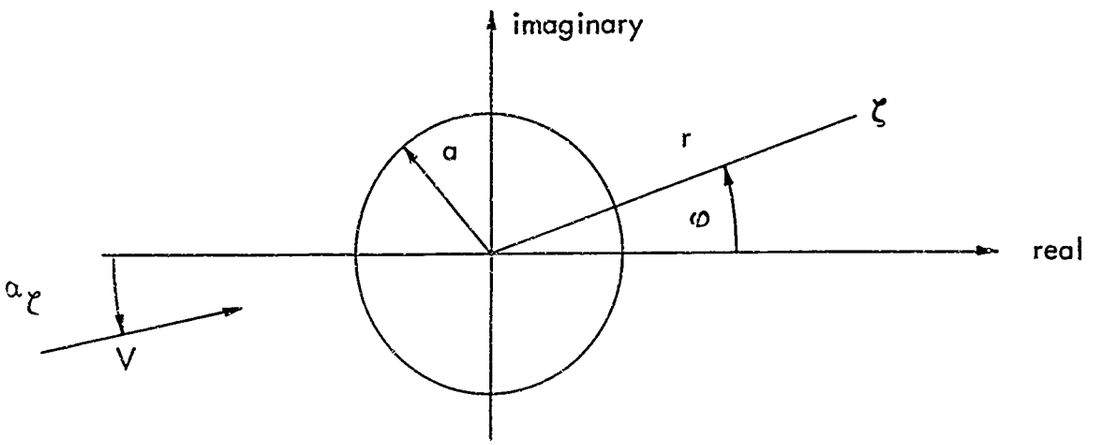

Substituting $\zeta = ae^{i\varphi}$, we obtain x and y on the profile as

$$x = A_{-1}\cos\varphi - B_{-1}\sin\varphi - A_o + \sum_1^\infty (A_n \cos n\varphi - B_n \sin n\varphi) \qquad [2]$$

$$Y = B_{-1}\cos\varphi - A_{-1}\sin\varphi - B_o + \sum_1^\infty (B_n \cos n\varphi - A_n \sin n\varphi) \qquad [3]$$

where the capital letter Y is used to denote points on the profile. To ensure that these expressions actually give the ordinates of the profile, the coefficients of the series must match a similar expansion for the profile coordinates. Usually we have $0 \leq x \leq 1$ and $Y = Y(x)$. In Appendix A, several foils are derived from exact theory. For foils which are slender in the horizontal direction, it is shown that x is

$$x = 1/2\,(1 - \cos\varphi) - 0(\tau, f)$$

where τ and f are the thickness ratio and camber ratio, respectively. For such slender foils, a slight change in the x value makes an even smaller change in the ordinate (except in regions of large curvature, e.g., the nose). With these facts in mind, we make the approximation* that

$$x = 1/2\,(1 + \cos\varphi) \qquad [4]$$

(note that this approximation reduces φ to a parameter) and $Y = Y(\varphi)$ where $Y(\varphi)$ is understood to be an implicit Fourier expansion, i.e.,

$$Y(\varphi) = a_o + \sum_1^\infty (a_n \cos n\varphi + b_n \sin n\varphi) \qquad [3a]$$

*Alternatively, this could be the starting point for an iteration leading to the exact transformation. However, the results show this approximation to be sufficiently accurate for the shapes considered here (see Appendix A).

Matching coefficients with Equation [3], we obtain

$$B_o = a_o = 1/2\pi \int_o^{2\pi} Y d\varphi$$

$$B_{-1} + B_1 = a_1 = 1/\pi \int_o^{2\pi} Y \cos\varphi \, d\varphi \,, \quad A_{-1} - A_1 = b_1 = 1/\pi \int_o^{2\pi} Y \sin\varphi \, d\varphi$$

$$B_n = a_n = 1/\pi \int_o^{2\pi} Y \cos n\varphi \, d\varphi \,, \qquad -A_n = b_n = 1/\pi \int_o^{2\pi} Y \sin n\varphi \, d\varphi$$

$$n \geq 2$$

Also, from Equation [4], we know that $A_o = 1/2$. Hence the coefficients are determined with the exception of A_{-1} and B_{-1}. Noting that the infinite series in Equations [2] and [3] are Fourier conjugates and that the A_{-1} and B_{-1} terms are not, we can immediately write an expression for determining these constants. However, the resulting expressions would involve A_o and B_o. The dependence on these coefficients may be eliminated by considering differentials of Equations [2] and [3]. Therefore, expressions which involve only A_{-1} and B_{-1} may be obtained by constructing the quantities:

$$T(\varphi) = dx/d\varphi - 1/2\pi \, \mathcal{P} \int_o^{2\pi} Y'(t) \cot(\varphi - t)/2 \, dt$$

$$S(\varphi) = dY/d\varphi + 1/2\pi \, \mathcal{P} \int_o^{2\pi} x'(t) \cot(\varphi - t)/2 \, dt \qquad [5]$$

where $\mathcal{P}$ indicates that the Cauchy Principle Value of the improper integral is to be taken and the primes denote differentiation with respect to the argument. Moriya's notation[5,10] differs from ours since he used the Fourier development which is more cumbersome than the integral and different al form presented here.

Substitution of the transformation equations (Equations [2] and [3]) into Equation [5] yields

$$T(\varphi) = -2\left[A_{-1}\sin\varphi + B_{-1}\cos\varphi\right]$$

$$S(\varphi) = 2\left[A_{-1}\cos\varphi - B_{-1}\sin\varphi\right] \qquad [5a]$$

With the given airfoil ordinates, the expressions for T and S are

$$T(\varphi) = -1/2\sin\varphi - 1/2\pi \int_0^{2\pi} Y'(t)\ \cot(\varphi - t)/2\ dt$$

$$S(\varphi) = 1/2\cos\varphi + Y'(\varphi) \qquad [6]$$

Equating Equations [5a] and [6] for $\varphi = 0$, we obtain

$$A_{-1} = 1/4\left[\ \right] + 2Y'(0)\ ]$$

$$B_{-1} = -1/4\pi \int_0^{2\pi} Y'(t)\ \cot\ t/2\ dt \qquad [7]$$

Note: $Y'(0) = (dY/d\varphi)_{\varphi=0} = -1/2\sin\varphi\,(dY/dx)_{TE}$ is zero, for example, with profiles having sharp trailing edges. Since not all profiles are of this form, $Y'(0)$ will be retained in the development.

Although the Fourier conjugates method is only one possible way of obtaining the coefficients, it is shown later that the group of coefficients $T(\varphi)$ and $S(\varphi)$ do appear in the expression for the velocity distribution. Even more important, we have found that other methods of obtaining only A_{-1} and B_{-1} do not give results which compare as favorably with exact results as do the $T(\varphi)$ and $S(\varphi)$ expressions.

LIFT COEFFICIENT

Arguments based on physical concepts lead to the conclusion that there is no flow around the trailing edge (Kutta condition). Thus, the numerical value of the circulation is just enough to place a stagnation point at the location on the circle which transforms to the trailing edge of the profile. In the exact transformation, the value of φ which makes x a maximum describes this location. In the approximation, the maximum value of x is at $\varphi = 0$.

The velocity in the circle plane is found by differentiating the complex potential $F(\zeta)$ with respect to ζ. For a circular cylinder inserted in a uniform stream such that the stream makes an angle α_ζ with the real axis, the complex potential is

$$F(\zeta) = V\left[\zeta e^{-i\alpha_\zeta} + a^2 e^{i\alpha_\zeta}/\zeta\right] + i(\Gamma/2\pi)\ln[\zeta/a]$$

where Γ is the circulation.

With ω as the independent variable, the velocity on the circular cylinder $\zeta = ae^{i\omega}$ becomes

$$dF/d\zeta\,|_{\zeta = ae^{i\omega}} = V\left[e^{-i\alpha_\zeta} - e^{i(\alpha_\zeta - 2\omega)}\right] + i(\Gamma/2\pi a)\, e^{-i\omega} \qquad [8]$$

Applying the Kutta condition, we put $dF/d\zeta = 0$ at $\zeta = a$, which sets

$$\Gamma = 4\pi a V \sin(\alpha_\zeta) \qquad [9]$$

Before the circulation can be converted to a lift coefficient, the effect of the mapping function on the free stream must be investigated. In the circle plane, the free stream velocity is given as

$$dF/d\zeta\,|_{\zeta \to \infty} \longrightarrow Ve^{-i\alpha_\zeta}$$

and in the profile plane as

$$dF/dz \Big|_{z \to \infty} = (dF/d\zeta) \,/\, (dz/d\zeta) \Big|_{\zeta \to \infty} \to V e^{-i\alpha_\zeta} a/C_{-1}$$

We define $$d\bar{F}/dz \Big|_{z \to \infty} \to U e^{-i\alpha}$$

and let $$C_{-1} = \kappa e^{i\chi} = K(\cos\chi + i \sin\chi)$$

But $$C_{-1} = A_{-1} + iB_{-1}$$

Thus $$K = \sqrt{A_{-1}^2 + B_{-1}^2}$$

$$\chi = \arctan \frac{B_{-1}}{A_{-1}} \qquad [10]$$

Equating the two descriptions for the freestream, we find

$$V = KU/a$$

$$\alpha_\zeta = \alpha - \chi \qquad [11]$$

With the above relations, the lift coefficient is found to be

$$C_L \equiv \frac{\rho U \Gamma}{1/2 \rho U^2 c} = 2\pi \sqrt{(4A_{-1})^2 + (4B_{-1})^2} \sin(\alpha - \chi) \qquad [12]$$

where c is the chord and ρ the fluid mass density. Hence, χ is the angle of zero lift in potential flow.

VELOCITY AND PRESSURE DISTRIBUTION

The velocity on the profile q is found by evaluating the expression

$$q = \left| \frac{dF\left(\zeta(z)\right)}{dz} \right|_{body} = \left| \frac{dF(\zeta)}{d\zeta} \Big/ \left(\frac{1}{a} \frac{dz}{d\omega}\right) \right|_{\zeta = ae^{i\varphi}}$$

Performing the operations, we find

$$q = \frac{2V a \left| \sin(\alpha_\zeta - \varphi) - \sin \alpha_\zeta \right|}{\sqrt{\left(\frac{dx}{d\omega}\right)^2 + \left(\frac{dY}{d\omega}\right)^2}} \qquad [13]$$

Substituting Equation [11] and expanding the right-hand side, we obtain

$$\frac{q}{U} = \frac{2}{\sqrt{\left(\frac{dx}{d\varphi}\right)^2 + \left(\frac{dY}{d\omega}\right)^2}} \left| (B_{-1} - B_{-1} \cos\varphi - A_{-1} \sin\omega) \cos\alpha \right.$$

$$\left. + (A_{-1} \cos\varphi - B_{-1} \sin\varphi - A_{-1}) \sin\alpha \right| \qquad [14]$$

The combination of transformation coefficients enclosed by parentheses is the previously defined $S(\varphi)$ and $T(\omega)$, Equation [5]. Hence, the expression for the nondimensional velocity can be written

$$\frac{q}{U} = \frac{\left| [T(\varphi) - T(0)] \cos\alpha + [S(\omega) - S(0)] \sin\alpha \right|}{\sqrt{1/4 \sin^2 \omega + Y'(\varphi)^2}}$$

$$\equiv \left| C(\varphi) \cos\alpha + D(\omega) \sin\alpha \right| \qquad [15]$$

where $T(\omega)$ and $S(\varphi)$ are given by Equations [6].

Since this method is for steady irrotational flow, Bernoulli's equation holds and gives the pressure distribution in coefficient form as

$$C_p \equiv \frac{P - P_\infty}{1/2\rho U^2} = 1 - \left(\frac{q}{U}\right)^2$$

EMPIRICAL MODIFICATION TO ACCOUNT FOR VISCOUS EFFECTS

In Reference 4, Pinkerton shows that an empirical modification to Theodorsen's exact potential theory[5] gives results which agree reasonably well with experimental measurements. In this chapter, we will show how Pinkerton's idea can be extended to the approximate potential theory just outlined.

Theodorsen[6] noted that conventional profiles are similar in shape and that application of the Jourkowski transformation to an arbitrary profile will yield a nearly circular shape of variable radius $1/4\ e^{\psi}$ and polar angle ω. The nearly circular shape can then be transformed into a circle of constant radius $1/4\ e^{\psi_o}$ and polar angle $\omega + \epsilon(\omega)$. With our notation and the circulation as yet unspecified, Theodorsen's expression for the velocity on the profile can be put in the form:

$$\frac{q}{U} = f(\varphi) \left| \sin(\alpha - \varphi - \epsilon) - \frac{\Gamma}{\pi e^{\psi_o} U} \right|$$

where

$$f(\varphi) = \frac{e^{\psi_o}\left[1 + \frac{d\epsilon}{d\varphi}\right]}{\sqrt{\left(1 + \left[\frac{d\psi}{d\omega}\right]\right)^2 \left(\sinh^2\psi + \sin^2\omega\right)}}$$

and

$$x = 1/2 \left[\cosh\psi_{LE} + \cosh\psi \cos\varphi\right]$$

$$Y = 1/2 \sinh\psi \sin\varphi$$

(Note that this φ is different from that used in the previous section.) The expressions for x and Y are sufficient to determine ψ and φ, and from these we can compute

$$\epsilon(\varphi) = 1/2\pi \int_0^{2\pi} \psi(t) \cot \frac{\varphi + \epsilon(\varphi) - [t + \epsilon(t)]}{2} \left[1 + \frac{d\epsilon}{dt}\right] dt$$

$$\psi_o = 1/2\pi \int_0^{2\pi} \psi(t) \left[1 + \frac{d\epsilon}{dt}\right] dt$$

Pinkerton's modification[6] is to add an arbitrary function to $\epsilon(\varphi)$. Arguing that the modification is a result of viscous effects and that the cumulative effect of the viscous forces are toward the trailing edge, he takes the addition to ϵ as

$$\alpha' = \Delta\alpha \left(\frac{1 + \cos\varphi}{2}\right)^R$$

where $\Delta\alpha$ is to be determined from the requirement that the lift be the experimental value and R is some constant $\geq 1/2$ (if $R < 1/2$ the velocity goes to infinity at the nose). Pinkerton considered only the case $R = 1$. Since ψ is the Fourier conjugate of ϵ, a change in ϵ would also cause a change in ψ. However, Pinkerton has found that the effect of this change in ψ is negligible in $f(\varphi)$.

For slender foils, both ϵ and ψ are small and we can approximate

$$x \approx 1/2 (1 + \cos\varphi)$$

$$Y \approx 1/2 \psi \sin\varphi$$

$$\left(1 + \frac{d\epsilon}{d\varphi} + \frac{d\alpha'}{d\varphi}\right) \approx \left(1 + \frac{d\epsilon}{d\varphi}\right)\left(1 + \frac{d\alpha'}{d\varphi}\right)$$

Thus the new expression for velocity is

$$\frac{q}{U} = f(\varphi) \left(1 + \frac{d\alpha'}{d\varphi}\right) \left| \sin\left[(\alpha - \alpha') - \varphi - \epsilon\right] - \sin(\alpha - \chi - \Delta\alpha) \right|$$

where $\chi = \epsilon(C)$ when the Kutta condition is satisfied. Comparing this expression with Equation [13], we can immediately write a similar modification to the

approximate theory given previously:

$$\frac{q}{U} = \frac{2K\left(1 + \frac{d\alpha'}{d\varphi}\right)\left| \sin(\alpha - \alpha' - \varphi - \chi) - \sin(\alpha - \chi - \Delta\alpha) \right|}{\sqrt{\frac{dx^2}{d\varphi} + \frac{dY^2}{d\varphi}}}$$

or

$$\frac{q}{U} = \left(1 + \frac{d\alpha'}{d\varphi}\right) \frac{\left| \begin{array}{l} T(\varphi)\cos(\alpha - \alpha') + S(\varphi)\sin(\alpha - \alpha') + \\ - \left[T(0)\cos(\alpha - \Delta\alpha) + S(0)\sin(\alpha - \Delta\alpha) \right] \end{array} \right|}{\sqrt{\frac{\sin^2\varphi}{4} + \frac{dY^2}{d\varphi}}} \qquad [16]$$

where $$\frac{d\alpha'}{d\varphi} = -\frac{\Delta\alpha}{2} \sin\varphi R\left(1 + \frac{\cos\varphi}{2}\right)^{R-1}$$

Except for notation, this is the solution obtained by Riegels.[7]

Implied in the above equation is that the lift coefficient is

$$C_L = 2\pi\sqrt{(4A_{-1})^2 + (4B_{-1})^2}\,\sin(\alpha - \chi - \Delta\alpha) \qquad [17]$$

We see at once that $\Delta\alpha$ is a fictitious decrease in the geometrical angle of attack to give the desired lift. This equation can be rearranged to give $\Delta\alpha$ in terms of an experimental lift coefficient

$$\Delta\alpha = \alpha - \chi - \arcsin \frac{C_{L_{(exp)}}}{2\pi\sqrt{(4A_{-1})^2 + (4B_{-1})^2}} \qquad [18]$$

With known values of the lift coefficient, this expression determines $\Delta\alpha$. Since we rarely have specific test data, a representative actual lift curve slope coefficient and angle of zero lift can be used to find the lift. Assuming these

values are known, we can determine the lift coefficient from the expression

$$C_L\Big|_{exp} = 2\pi(\alpha - \alpha_{o_e}) \qquad [19]$$

where π is equal to $dC_L/d\alpha\,|_{exp}/2\pi$ and α_{o_e} is the experimental angle of zero lift. (π and α_{o_e} are discussed further later in the paper.)

In order to more clearly show the effect of $\Delta\alpha$, the velocity distribution will be linearized on $\Delta\alpha$. This will be put in the form of the potential velocity plus a term multiplied by $\Delta\alpha$. The linearization is performed by replacing $\sin\alpha'$ by α' and $\cos\alpha'$ by 1. Ignoring all small quantities multiplied by α', we find*

$$\frac{q}{U} = \left(1 + \frac{d\alpha'}{d\varphi}\right)\left[\frac{q}{U}\right]_{\Delta\alpha = 0} \qquad E(\varphi) \qquad [20]$$

where $$E(\varphi) = (1/2)\,\frac{1 - x^R}{\sqrt{1/4\,\sin^2\sigma + Y'(\varphi)^2}} - x^R\,D(\varphi)$$

and $\left(\frac{q}{U}\right)_{\Delta\alpha = 0}$ is the potential velocity. In addition to showing the effect of $\Delta\alpha$ on the potential velocity, this expression is easier for hand calculations with the potential theory known.

NUMERICAL METHOD

TRIGONOMETRIC SERIES TO REPRESENT THE ORDINATES

To use Equation [16], we need an analytical expression for the ordinates. For tabulated offsets, this means either constructing a Fourier series or curve fitting a polynomial to the ordinates. As will be shown in this section, a trigonometric

*With R = 1, the linearized expression for velocity would be the same as that obtained by Riegels[7] in 1943 if he had recognized that $C(\sigma)\sin\alpha$ in our $E(\varphi)$ term is small in the normal incidence angle.

series may be fitted analytically to ordinates given at certain specific stations along the chord. The slope and cotangent integral then become a summation of the product of constant coefficients and the ordinates at these fixed stations.

The formulas used to approximate the ordinates can be developed by either the least-square-error approach[11] or by requiring the series to pass through the given points.[12] Both methods are equivalent so we will outline the more direct method of curve fitting through the given points.

Values for the ordinates are required at $2N + 1$ equally spaced values of φ between 0 and 2π in Equation [4], i.e., at the fixed stations

$$x_m = \frac{1 + \cos \varphi_m}{2} = \frac{1 + \cos \frac{m\pi}{N}}{2} \quad , \; 0 \leq m \leq 2N \qquad [21]$$

Although we have $2N + 1$ values of the ordinates, only $2N$ are independent since the periodicity requires $Y(0) = Y(2\pi)$, or the mean value if there is a discontinuity at the trailing edge. Noting that $\sin N\varphi_m$ is zero at all m, we see that Equation [3a] should be truncated to the $2N$ terms

$$Y(\varphi) = a_o + \sum_{1}^{N-1} (a_n \cos n\varphi + b_n \sin n\varphi) + a_N \cos N\varphi$$

Setting this expression equal to the $2N$ independent ordinates, we obtain a system of linear equations to be solved for the coefficients:

$$Y_m = a_o + \sum_{1}^{N-1} (a_n \cos n\varphi_m + b_n \sin n\varphi_m) + a_N \cos N\varphi_m$$

These equations are solved by multiplying both sides of the above equation by the multiple of the desired coefficient and summing from zero to $2N - 1$. Using this

approach we obtain the constants

$$a_o = \frac{1}{2N} \sum_{0}^{2N-1} Y_m$$

$$a_n = \frac{1}{N} \sum_{0}^{2N-1} Y_m \cos \frac{mn\pi}{N} \qquad b_n = \frac{1}{N} \sum_{0}^{2N-1} Y_m \sin \frac{mn\pi}{N}$$

$$a_N = \frac{1}{2N} \sum_{0}^{2N-1} Y_m \cos m\pi$$

(Note that for $n < N$, these expressions are identical with results of evaluating integral expressions for the Fourier constants by the trapezoidal rule with equal angular spacing as above.) With $Y(0) = 0 = Y(\pi)$, the expression for the ordinates, Equation (3a), becomes

$$Y(\varphi) = Y_{odd}(\varphi) + Y_{even}(\varphi) \tag{22}$$

where

$$Y_{odd}(\varphi) = \sum_{1}^{N-1} b_n \sin n\varphi = \frac{1}{N} \sum_{m=1}^{N-1} (Y_m - Y_{2N-m}) \sum_{n=1}^{N-1} \sin n\varphi_m \sin n\varphi \tag{23}$$

$$Y_{even}(\varphi) = \sum_{0}^{N} a_n \cos n\varphi = \frac{1}{N} \sum_{m=1}^{N-1} (Y_m + Y_{2N-m}) \left[\sum_{n=1}^{N-1} \cos n\varphi_m \cos n\varphi + \frac{1 + \cos N\varphi_m \cos N\varphi}{2} \right] \tag{24}$$

and Y_m and Y_{2N-m} are the upper and lower surface ordinates, respectively, measured from the nose-tail line at $\varphi = \varphi_m = \frac{m\pi}{N}$.

The odd part of the series arises from thickness and the even part from camber. It should be noted that the odd function given above assumes a rounded leading and

trailing edge and the even function assumes finite slope $\frac{d(Y_m + Y_{2N-m})}{dx}$ at the leading and trailing edges.

EVALUATION AT SPECIFIED POINTS

The troublesome expressions in T (φ) and S (φ) (Equation [6]) are the singular corangent integral and the slope, respectively. Using the numerical expressions for Y (φ), we can easily perform the necessary operations. The expressions will involve a double summation as in the Y (φ) expression. Since the summation involving the trigonometric terms is to only a finite limit, the sum may be calculated analytically.* At a point corresponding to an input point ($\varphi = \varphi_\nu = \frac{\nu\pi}{N}$, ν one of the m), the cotangent integral reduces to

$$1/2\pi \oint_0^{2\pi} Y'(t) \cot\frac{\varphi_\nu - t}{2}\, dt = 1/2N \sum_{m=1}^{N-1} \left[1 - (-1)^{m+\nu}\right] \left[\frac{Y_m}{\cos\frac{m-\nu}{N}\pi - 1} + \frac{Y_{2N-m}}{\cos\frac{m+\nu}{N}\pi - 1}\right]$$

(for $m = \nu$, the multiple of Y_m is easily shown to equal $N/2$).

Similarly, the slope (in the φ plane) reduces to

$$\left.\frac{dY}{d\varphi}\right)_{\varphi = \varphi_\nu} = 1/2 \sum_{m=1}^{N-1} (-1)^{1+m+\nu} \left[Y_m \cot\frac{(m-\nu)\pi}{2N} - Y_{2N-m}\cot\frac{(m+\nu)\pi}{2N}\right]$$

(for $m = \nu$, the multiple of Y_m is zero).

The numerical expressions of Riegels[7] may be added together to obtain these results. However, these equations require computation of a N + 1 by N - 1 array of coefficients;

*See, for example, References 13 and 14.

this is a lengthy calculation either by hand or on a high-speed computer. Further simplification is possible if we define $\lambda = m - \nu$ in the first term of summation and $\lambda = m + \nu$ in the second. The equations then reduce to

$$1/2 - \frac{1}{\pi} Y'(t) \cot \frac{\varphi_\nu - t}{2}\, dt = \frac{N}{2} Y_\nu + \frac{1}{2N} \sum_{\lambda=1}^{N-1} \left[Y_{\nu+\lambda} + Y_{\nu-\lambda} \right] \frac{1 - (-1)^\lambda}{\cos \frac{\lambda\pi}{N} - 1} \qquad [25]$$

$$\left.\frac{dY}{d\varphi}\right|_{\varphi_\nu} = 1/2 \sum_{\lambda=1}^{N-1} \left[Y_{\nu+\lambda} - Y_{\nu-\lambda} \right] (-1)^{\lambda+1} \cot \frac{\lambda\pi}{2N} \qquad [26]$$

where we understand that $Y_{-m} = Y_{2N-m}$ and $Y_{2N+m} = Y_m$.

These expressions are now quite simple and can easily be set up for hand or computer calculations with a minimum of calculations. It is necessary that only the ordinates be cyclically rearranged before each computation.

The expressions for $T(\varphi)$ and $S(\varphi)$ at $\varphi = \varphi_\nu$ are now

$$T_\nu \equiv T(\varphi_\nu) = -1/2 \left[\sin \frac{\nu\pi}{N} + N Y_\nu - \frac{1}{N} \sum_{\lambda=1}^{N-1} \left(Y_{\nu+\lambda} + Y_{\nu-\lambda} \right) \frac{1 - (-1)^\lambda}{1 - \cos \frac{\lambda\pi}{N}} \right] \qquad [27]$$

$$S_\nu \equiv S(\varphi_\nu) = 1/2 \left[\cos \frac{\nu\pi}{N} + \sum_{\lambda=1}^{N-1} \left(Y_{\nu-\lambda} - Y_{\nu+\lambda} \right) (-1)^\lambda \cot \frac{\lambda\pi}{2N} \right] \qquad [28]$$

and the modified velocity at $\varphi = \varphi_\nu$ is

$$\left.\frac{q}{U}\right|_{\varphi_\nu} = \frac{\left| \begin{array}{l} T_\nu \cos(\alpha - \alpha') + S_\nu \sin(\alpha - \alpha') \\ -\left[T_0 \cos(\alpha - {}^{\prime}\alpha) + S_0 \sin(\alpha - {}^{\prime}\alpha) \right] \end{array} \right|}{\sqrt{1/4 \sin^2 \frac{\nu\pi}{N} + \left.\frac{dY}{d\varphi}\right|_{\varphi_\nu}^2}} \times$$

$$\left[1 - \frac{\Delta\varphi}{2} \sin \frac{\nu\pi}{N} \; R \left(\frac{1 + \cos \frac{\nu\pi}{N}}{2} \right)^{R-1} \right] \qquad [16a]$$

EVALUATION AT AN ARBITRARY POINT

As mentioned in the Introduction, the motivation for this research is to obtain the minimum pressure. Unfortunately, there is no guarantee that the pressure distribution computed at the fixed points will yield the minimum value. If we note that only when the minimum is near the nose does the pressure distribution have a steep gradient, then our problem can be reduced to obtaining more data just near the nose.

The procedure outlined for obtaining the slope and cotangent integral at specified points can be followed for an arbitrary φ value. The expressions obtained are more complicated but still give a single summation of the ordinates at the input points and trigonometric expressions which can be evaluated once and for all at any desired point. Although the results appear to be new, the derivation is not sufficiently involved to warrant presentation and we give only the final results:

$$
\begin{aligned}
1/2\pi \int_0^{2\pi} Y'(t) \cot\frac{\varphi - t}{2}\, dt
&= \sum_{m=1}^{N-1} (Y_m - Y_{2N-m}) \left[\frac{(-1)^m \cos N\varphi - 1}{2N} \cdot \frac{\sin\varphi_m \sin\varphi}{(\cos\varphi - \cos\varphi_m)^2} \right. \\
&\quad \left. + \frac{(-1)^{m+1} \sin N\varphi}{2} \cdot \frac{\sin\varphi_m}{\cos\varphi - \cos\varphi_m} \right] \\
&\quad + \sum_{m=1}^{N-1} (Y_m + Y_{2N-m}) \left[\frac{(-1)^m \cos N\varphi - 1}{2N} \cdot \frac{1 - \cos\varphi_m \cos\varphi}{(\cos\varphi - \cos\varphi_m)^2} \right. \\
&\quad \left. + \frac{(-1)^{m+1} \sin N\varphi}{2} \cdot \frac{\sin\varphi}{\cos\varphi - \cos\varphi_m} \right] \qquad [29]
\end{aligned}
$$

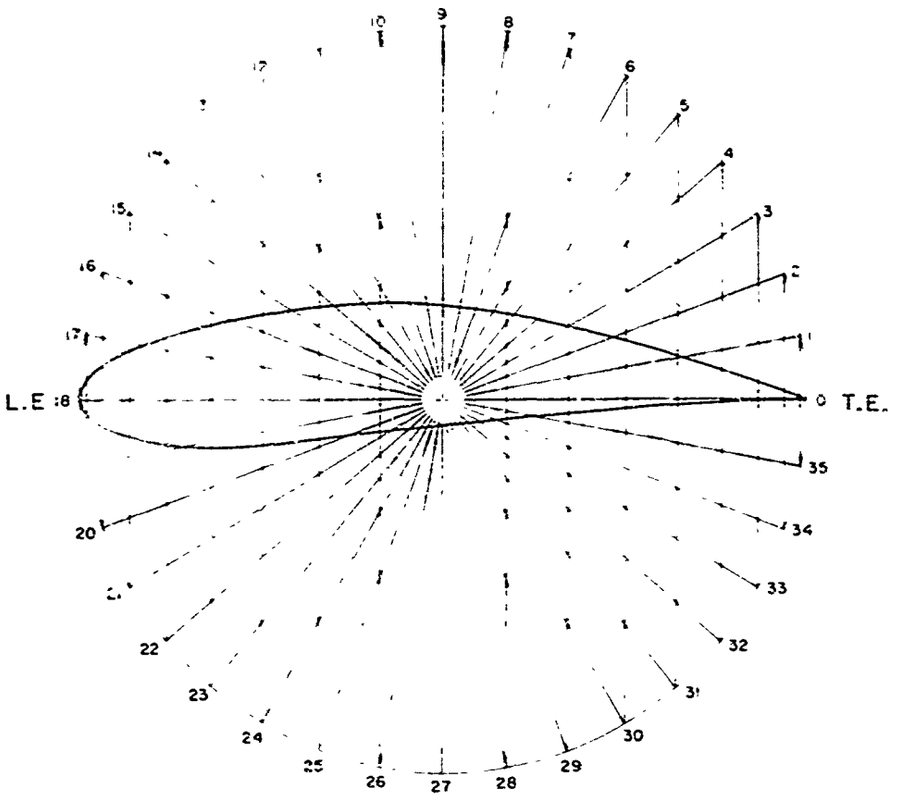

Figure 1 – Chordwise Stations $x_m = 1/2\ (1 + \cos m\pi/18)$

TABLE 1

Values of $x_m = 1/2(1 + \cos m\pi/18)$

m	ϕ, deg	x
0	0	1.0
1	10	0.992404
2	20	0.969846
3	30	0.933013
4	40	0.883022
5	50	0.821394
6	60	0.75
7	70	0.671010
8	80	0.586824
9	90	0.5
10	100	0 413176
11	110	0.328990
12	120	0 25
13	130	0 178606
14	140	0 116978
15	150	0 066987
16	160	0 030154
17	170	0 007596
18	180	0

x_{36-m} x_m

$$\frac{dY}{d\varphi} = \sum_{m=1}^{N-1} (Y_m - Y_{2N-m}) \left[\frac{(-1)^{m+1} \sin N\varphi}{2N} \cdot \frac{\sin\varphi_m \sin\varphi}{(\cos\varphi - \cos\varphi_m)^2} \right.$$

$$\left. + \frac{(-1)^{m+1} \cos N\varphi}{2} \cdot \frac{\sin\varphi_m}{\cos\varphi - \cos\varphi_m} \right]$$

$$+ \sum_{m=1}^{N-1} (Y_m + Y_{2N-m}) \left[\frac{(-1)^{m+1} \sin N\varphi}{2N} \cdot \frac{1 - \cos\varphi_m \cos\varphi}{(\cos\varphi - \cos\varphi_m)^2} \right.$$

$$\left. + \frac{(-1)^{m+1} \cos N\varphi}{2} \cdot \frac{\sin\varphi}{\cos\varphi - \cos\varphi_m} \right] \qquad [30]$$

In order to obtain a better estimate of the minimum pressure, the velocity is evaluated at additional points near the nose using these expressions. Choice of these additional points depends upon the choice of N. In the pressure program, N will be 18, so that φ increases in increments of 10 degrees; see Figure 1 and Table 1. The intermediate points selected are listed in Table 2. They are each integer degrees between the nose ($\varphi=\pi$) and the input point on each side of it ($\varphi = \pi \pm \frac{\pi}{18}$) and three additional points 2 1/2 degrees apart between this point ($\varphi=\pi \pm \frac{\pi}{18}$) and its neighbor ($\varphi = \pi \pm \frac{\pi}{9}$).

COMPARISONS WITH ANALYTICAL RESULTS

The numerical expressions for the ordinates are obtained by forcing the expression to pass through specified points. Thus there is no assurance that the computations will be reasonable between the points. Also, we have assumed that a

finer spacing of computed data near the nose is sufficient to determine the minimum pressure. We cannot check these problems in a general sense, but we can make comparisons in specific cases.

In order to check the accuracy of the numerical solution, the computations were performed both analytically and numerically for the linearized symmetrical Joukowski profile[13]

$$x = 1/2\,(1 + \cos\varphi)$$

$$Y_T = \frac{2\tau}{3\sqrt{3}}\,(\sin\varphi - 1/2 \sin 2\varphi)$$

added to the parabolic camberline[13]

$$Y_c = f \sin^2 \varphi$$

where τ is the thickness ratio and f is the camber ratio. The analytical and numerical solutions were accurate to at least four significant figures when the input was specified to five significant figures. This accuracy is more than adequate for any practical use.

In order to make a comparison with the minimum pressure computed analytically and numerically at discrete points, the results for a symmetrical ellipse were used. For this simple shape, the location and the value of the minimum pressure are easily obtained analytically. From the exact potential velocity distribution (see Appendix A), we obtain the location of maximum velocity $\left(\frac{dq}{d\rho} = 0\right)$ from the following equation

$$\tan\varphi = \frac{\tau^2}{\sin\rho(1 - \tau^2) - \tan\rho}$$

where τ is the thickness ratio. Particular σ values can be selected and the angle of incidence for maximum velocity calculated from this equation. A graphical comparison of both the location and value of the maximum velocity as computed analytically and numerically at the fixed points is given in Figure 2 for thickness ratios of 0.05 and 0.1. This comparison shows that even though the location in the nose region may be off somewhat, the velocity is calculated with sufficient accuracy.

COMPUTER PROGRAM

A computer program has been written for calculating the pressure distribution by the numerical method outlined in the previous section. The FORTRAN statements of the source program are listed in Appendix C. These statements are for Applied Mathematics Laboratory Problem 840-041-F.

The order of the computer operations is as follows: First, the constant coefficients in Equations [27] through [30] and other constants are calculated and stored. Then the input data are read and the summed products of the ordinates and the stored constants obtained. Finally, for each angle of attack, the pressure distribution at the input points and at the intermediate points is determined from Equation [16] (actually Equation [16a] of the numerical method) with $\alpha' = \Delta\alpha x$ (i.e., R = 1). Since the last operation performed is for the angle of attack, variations in angle of attack take least machine time.

The data needed to compute the pressure distribution consist of the angles, in degrees, for which the pressure distribution is desired; estimates of the angle of zero lift,* in degrees, and an average lift-curve slope coefficient* $\eta = \left.\frac{dC_L}{d\alpha}\right)_{exp} / 2\pi$

*Reference 15 finds that η is primarily a function of the thickness form and that α_{o_e} is primarily a function of the meanline. Tabulated values for many sections can be found in Reference 16. As shown by the data in Reference 16, both η and α_{o_e} are functions of the Reynolds number.

TABLE 2

Intermediate Points

$\pm(\theta - \pi)$, deg.	x
1	0.000076
2	0.000305
3	0.000685
4	0.001218
5	0.001902
6	0.002739
7	0.003727
8	0.004866
9	0.006156
12.5	0.011852
15	0.017037
17.5	0.023142

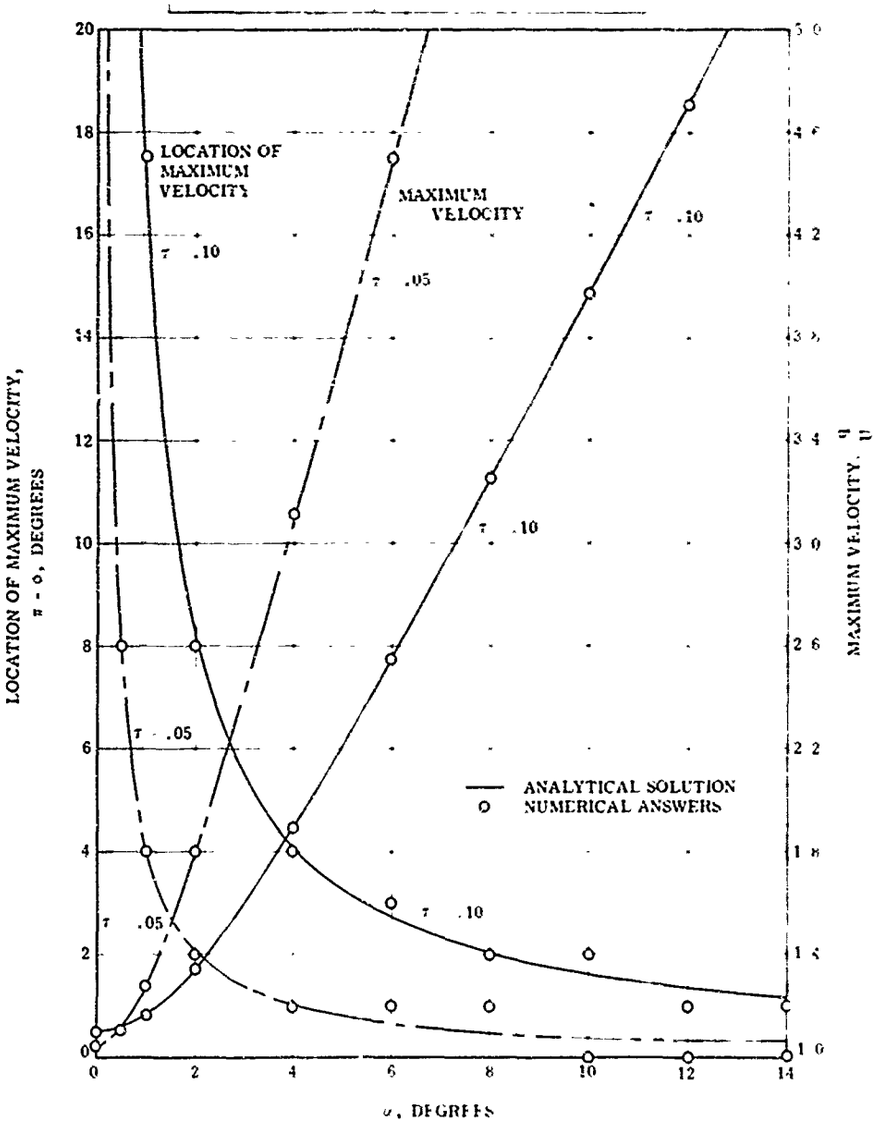

Figure 2 – Comparison of Analytical and Numerical Solutions for the Location and Value of the Maximum Velocity on Ellipses

for use in Equation [19]; and, of course, the airfoil ordinates, in fractions of the chord. The nondimensional ordinates should be accurate to about one-tenth of 1 percent of the maximum ordinate to give a smooth pressure curve. (Accuracy to four decimal places is usually suificient.)

The stations for whicl the offsets are required in the numerical method are given by Equation [21], shown in Figure 1, and tabulated in Table 1. Since these stations are often inconvenient to use with tabulated data, provision for input at arbitrary x values is also provided. The input at the required stations is obtained from a third-degree polynomial fitted through four ordinates, two on each side of the required station. The interpolation is performed between angular stations since the ordinates do not then have an infinite slope at the leading edge (see, e.g., Figure 10). The arbitrary stations should be as near the required values as possible. This is especially important at the leading and trailing edges.

As mentioned, several input options are provided. As with all machine computations, input must be given in a nonvarying manner; hence the input descriptions must be rigidly followed.

Option 1: Ordinates at Required Stations

The shortest method of data input is to specify ordinates at the required stations. This type of input naturally results in the shortest running time since no interpolation for the ordinates is required. The necessary order of input is shown in Figure 3a where each horizontal block represents a different card starting from Column 1. However, not all the cards indicated for the angles of attack and the ordinates

should be filled; only as many boxes as are needed should be used. (See the sample input, Figure 3b.) When several profiles are given for the same angles of attack, it is important that only similar types of profiles be grouped together (i.e., either symmetric thickness forms or nonsymmetric cambered foils, not both). When changing types of foils, a new set of input, starting with the initial control card for the angles, is necessary. Additional members of a group of profiles require only the cards indicated under PROFILE INFORMATION in Figure 3a.

Option 2: Ordinates at Arbitrary Stations

As mentioned, input may also be given at arbitrary stations. Two sub-options are considered in this case.

(a) Points on Profile

The first of these sub-options is to specify points (x, Y) around the foil in the direction of increasing m (see Figure 1). The upper surface trailing edge ordinate must be the first point specified and the lower surface trailing edge ordinate must be the last point given.* The nose (see Equation [B2] in Appendix B) must also be given before the input points. In addition, the nose point should be given again, in order, midway in the listing of coordinates. The program shrinks and rotates the coordinates to put the nose at (0,0) since this orientation has been found to be the most accurate. (This point is further discussed in Appendix B.) The rotation angle is added to each of the input angles so that α is measured from the original reference line. A maximum of 53 points is permitted.

*Even though there are provisions for inserting ordinates at the trailing edge, and though they are printed out in the pressure program, no use is made of them when computing the pressure distribution. They are used in the interpolation and hence should not be omitted when using the arbitrary input option.

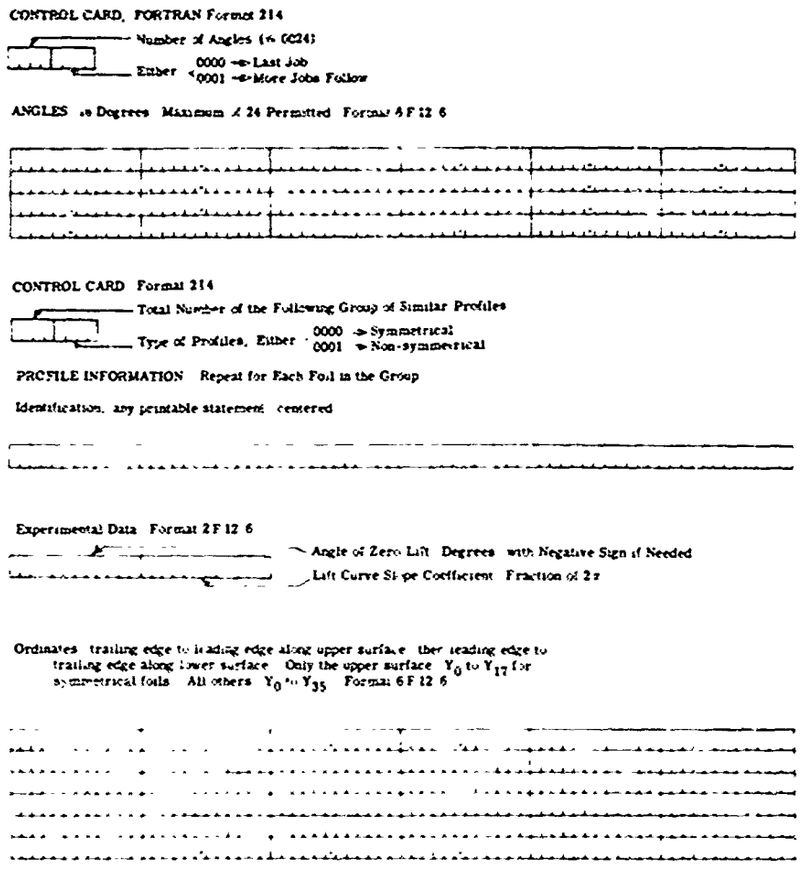

Figure 3a – Format for Data Input to Computer Program at Required Stations

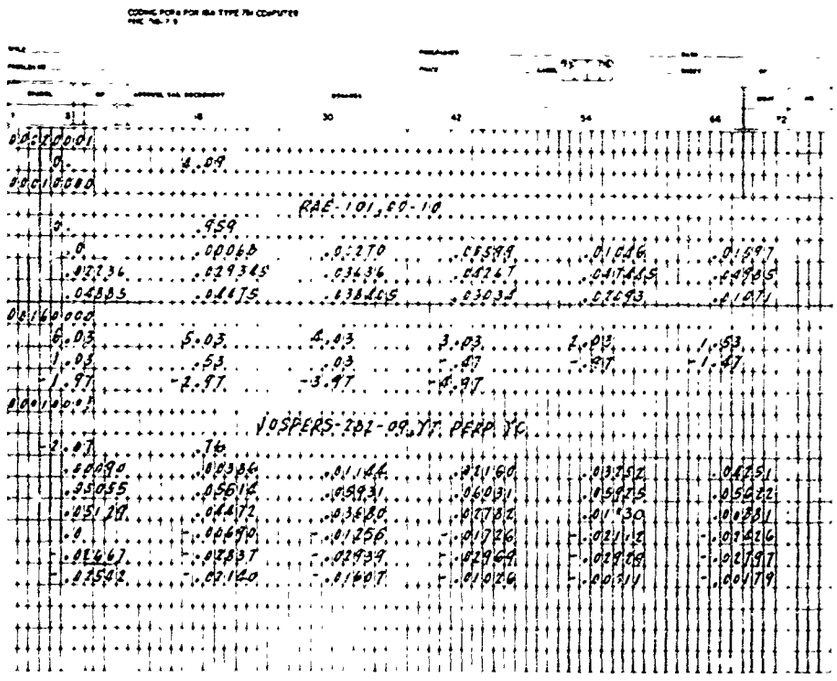

Figure 3b – Sample Input at Required Stations

Figure 3 – Data Input to Computer at Required Stations

(b) Values of Thickness, Camber, and Camberline Slope

The second sub-option is to give values of the station, the thickness, the camber, and the camberline slope from trailing edge to leading edge. These quantities are combined in the NACA manner[7] (thickness applied perpendicular to the camber) to obtain the coordinates of the foil (see page 113 of Reference 15 and also Equation [B1] in Appendix B of this report). The coordinates are rotated and shrunk as above. If the surface is to be computed by $Y = Y_c \pm Y_t$, the camberline slope should be entered as zero in the input and the nose radius is not needed. Input at 27 stations is permitted.

The format for data input in both cases above is shown in Figure 4a, and sample input in Figure 4b.

Other Options

Although not shown in Figures 3a and 4a, if a 1 is placed in Column 16 of the control card just before the PROFILE INFORMATION cards, values of the lift coefficient (as many as the angles and the same format) may be given in place of the angle of zero lift and lift-curve slope coefficient. (See the sample input, Figure 4b.) Note that lift coefficients must be given for each profile grouped under this control card. Also, if a 1 is placed in Column 12 of the initial control card, only values of the angle of attack, lift coefficient, minimum pressure coefficient, maximum velocity, x location, and integrated moment coefficient about the line x = 0.25 are printed out instead of the complete pressure distribution around the foil. There is a considerable saving in paper and computer time when using this option.

Figure 4 – Data Input to Computer at Arbitrary Stations

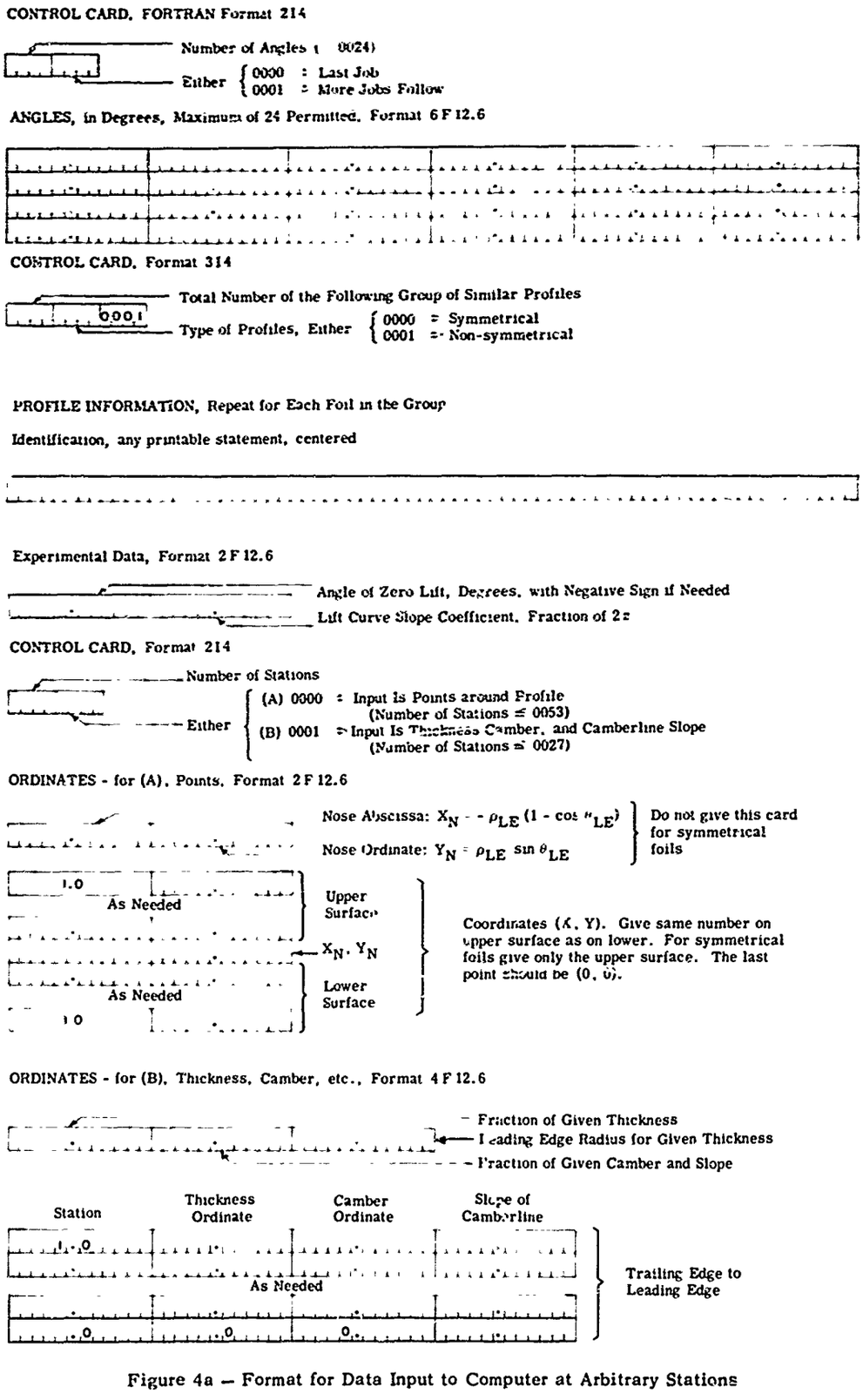

Figure 4a – Format for Data Input to Computer at Arbitrary Stations

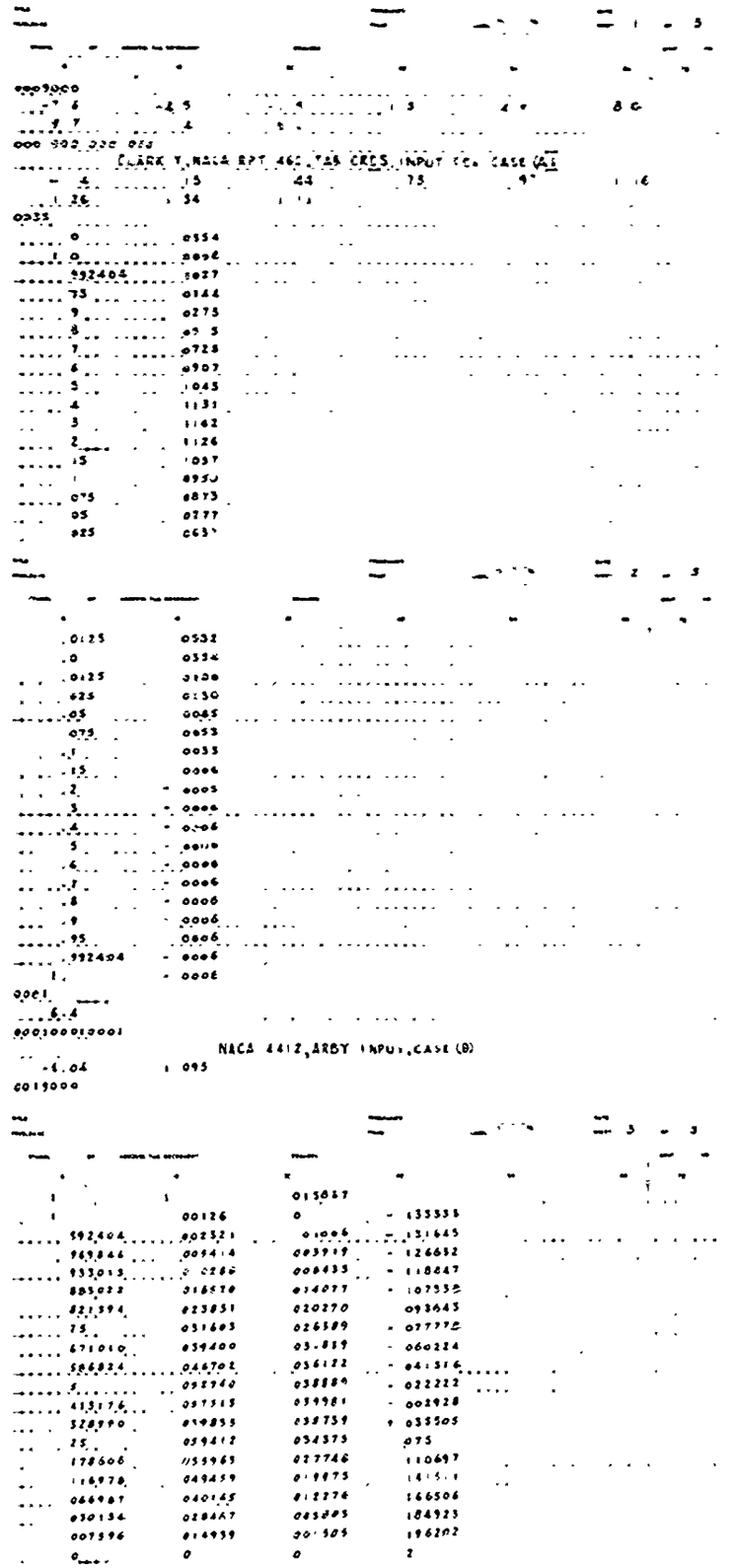

Figure 4b – Sample Input at Arbitrary Stations

Sample output for the RAE 101 (10-percent thickness) is shown in Figures 5 and 6. This is the data plotted in Figure 15. The first two pages of output (Figure 5) for each set of ordinates are titled Profile Constants. The first page includes the stations (column headed X) and the ordinates (column headed Y). The column headed C is the velocity distribution on the profile at zero angle of attack and the column headed D is the velocity distribution due to the angle of attack (Equation [15]). The column headed E is a factor necessary to find the modified, linearized pressure distribution (see Equation [20]). These three columns permit rapid evaluation by hand of the velocity at other than the input angles without rerunning the data. (At the bottom of the page is an expression which shows how to combine Columns C, D, and E to obtain the linearized pressure distribution.) The last column is $\frac{dY}{d\varphi} = -1/2 \sin\varphi \cdot \frac{dY}{dx}$. The theoretical slope factor $\frac{dC_L}{d\alpha} / 2\pi \Big|_{C_L = 0}$ is printed out at the bottom of the page as well as the theoretical angle of zero lift.

Additional information may be obtained from the data on the Profile Constants page of output. The angle of attack at which a stagnation point lies at the nose,* $(q)_{\varphi = \pi, \angle\alpha = 0} = 0$, may be calculated for potential flow from Equation [15]:

$$C(\pi) \cos\alpha + D(\pi) \sin\alpha = 0$$

i.e.,

$$\alpha = \arctan - \frac{C(\pi)}{D(\pi)}$$

For $\Delta\alpha \neq 0$, the nose stagnation angle may be similarly obtained from the linearized

*This angle is not the same as Theodorsen's ideal angle of attack.[6] The ideal angle (for thick foils) is defined as the angle of which a stagnation point lies at the forward end of the camberline. As noted by Theodorsen, this angle is of limited practical importance.

AML PROBLEM 840-041.ARBITRARY AIRFOIL PRESSURE DISTRIBUTION
WITH EMPIRICAL CORRECTION FOR VISCOSITY

PROFILE CONSTANTS

RAE-101-010

X	Y	C	D	E	DY/DPHI
1.000000	-0.	-0.	-0.	0.	0.001998
0.992434	0.000680	0.890691	0.026481	-0.069871	0.007287
0.969846	0.002700	0.933471	0.096858	-0.181740	0.015520
0.933013	0.005990	0.958660	0.186467	-0.307426	0.022185
0.883022	0.010460	0.978938	0.279256	-0.427845	0.028863
0.821394	0.015970	0.997232	0.380868	-0.545076	0.034145
0.750000	0.022360	1.016276	0.490314	-0.655257	0.038834
0.671010	0.029345	1.038498	0.615677	-0.761927	0.040635
0.586824	0.036360	1.062834	0.761407	-0.865047	0.039075
0.500000	0.042670	1.088804	0.937296	-0.967603	0.032369
0.413176	0.047445	1.114414	1.150647	-1.070719	0.021690
0.328990	0.049850	1.139587	1.422610	-1.182065	0.004568
0.250000	0.048850	1.167911	1.771429	-1.308325	-0.015548
0.178606	0.044750	1.144379	2.222439	-1.465799	-0.030556
0.116978	0.038405	1.137954	2.859395	-1.696827	-0.041660
0.066987	0.030340	1.125485	3.863976	-2.087953	-0.050476
0.030154	0.020930	1.087641	5.708723	-2.863493	-0.056763
0.007596	0.010710	0.945092	9.983661	-4.773448	-0.060158
0.	0.	-0.	17.144991	-8.056399	-0.062062
0.007596	-0.010710	-0.945092	9.983661	-4.773448	-0.060158
0.030154	-0.020930	-1.087641	5.708723	-2.863493	-0.056743
0.066987	-0.030340	-1.125485	3.863976	-2.087953	-0.050476
0.116978	-0.038405	-1.137954	2.859395	-1.696827	-0.041660
0.178606	-0.044750	-1.144379	2.222439	-1.465799	-0.030556
0.250000	-0.048850	-1.167911	1.771429	-1.308325	-0.015548
0.328990	-0.049850	-1.139587	1.422610	-1.182065	0.004568
0.413176	-0.047445	-1.114414	1.150647	-1.070719	0.021690
0.500000	-0.042670	-1.088804	0.937296	-0.967603	0.032369
0.586824	-0.036360	-1.062834	0.761407	-0.865047	0.039075
0.671010	-0.029345	-1.038498	0.615677	-0.761927	0.040635
0.750000	-0.022360	-1.016276	0.490314	-0.655257	0.038834
0.821394	-0.015970	-0.997232	0.380868	-0.545076	0.034145
0.883022	-0.010460	-0.978938	0.279256	-0.427845	0.028863
0.933013	-0.005990	-0.958660	0.186467	-0.307426	0.022185
0.969846	-0.002700	-0.933471	0.096858	-0.181740	0.015520
0.992434	-0.000680	-0.890691	0.026481	-0.069871	0.007287
1.000000	-0.	-0.	-0.	0.	0.001998

NON-DIMENSIONAL VELOCITY
V=(C*COS(ALFA)+D*SIN(ALFA))*(1-/+DELTA*SQRT(4-X**2))+DELTA*E

DCL/D(ALPHA)/2PI (THEORY)= 1.003996
ANGLE,CL=0 (THEORY) = 0. DEG

NOTE,TE ORDINATE NOT USED INTERNALLY

AML PROBLEM 840-041.ARBITRARY AIRFOIL PRESSURE DISTRIBUTION
WITH EMPIRICAL CORRECTION FOR VISCOSITY

PROFILE CONSTANTS

RAE-101-010

INTERMEDIATE VALUES

UPPER SURFACE

X	C	D	E	DY/DPHI
0.000076	0.161276	16.982900	-7.981671	-0.062038
0.000305	0.313757	16.522598	-7.769532	-0.061966
0.000685	0.450819	15.831151	-7.451068	-0.061848
0.001218	0.569054	14.992645	-7.065237	-0.061689
0.001903	0.667997	14.085385	-6.648289	-0.061492
0.002739	0.749135	13.169452	-6.228003	-0.061265
0.003727	0.814890	12.284467	-5.822653	-0.061012
0.004866	0.867892	11.452906	-5.442567	-0.060740
0.006156	0.910580	10.685003	-5.092397	-0.060456
0.011852	1.005922	8.501872	-4.103034	-0.059397
0.017037	1.043992	7.385886	-3.584795	-0.058605
0.023142	1.069452	6.436098	-3.181521	-0.057745

LOWER SURFACE

X	C	D	E	DY/DPHI
0.000076	-0.161276	16.982900	-7.981671	-0.062038
0.000305	-0.313757	16.522598	-7.769532	-0.061966
0.000685	-0.450819	15.831151	-7.451068	-0.061848
0.001218	-0.569054	14.992645	-7.065237	-0.061689
0.001903	-0.667997	14.085385	-6.648289	-0.061492
0.002739	-0.749135	13.169452	-6.228003	-0.061265
0.003727	-0.814890	12.284467	-5.822653	-0.061012
0.004866	-0.867892	11.452906	-5.442567	-0.060740
0.006156	-0.910580	10.685003	-5.092397	-0.060456
0.011852	-1.005922	8.501872	-4.103034	-0.059397
0.017037	-1.043992	7.385886	-3.584795	-0.058605
0.023142	-1.069452	6.436098	-3.181521	-0.057745

Figure 5 – Typical Output from Computer, Profile Constants

AML PROBLEM 840-041.ARBITRARY AIRFOIL PRESSURE DISTRIBUTION
WITH EMPIRICAL CORRECTION FOR VISCOSITY

PRESSURE DISTRIBUTION

RAE-101-010

SYMMETRICAL PROFILE

ALFA	CL	DELTA	SIN(ALFA)	LIFT SLOPE	ALFA,CL=0
4.090000	0.430129	0.003146	0.071323	0.959000	-0.

X	POTNL VELOC	VISC INCRM	VISC VELOC	POTNL P/Q	VISC P/Q
1.000000	0.	0.	0.	1.000000	1.000000
0.992404	0.890311	-0.000269	0.890042	0.207346	0.207825
0.969846	0.938002	-0.000877	0.937124	0.120153	0.121798
0.933013	0.969538	-0.001532	0.966006	0.059997	0.062965
0.883022	0.996361	-0.002161	0.994202	0.007261	0.011563
0.821394	1.017857	-0.002763	1.019094	-0.044191	-0.038552
0.750000	1.048659	-0.003318	1.045341	-0.099686	-0.092738
0.671010	1.079765	-0.003835	1.075931	-0.165893	-0.157627
0.586824	1.114633	-0.004305	1.110128	-0.241960	-0.232384
0.500000	1.152883	-0.004731	1.148151	-0.329138	-0.318251
0.413176	1.193643	-0.005110	1.188534	-0.424784	-0.412642
0.328990	1.238150	-0.005460	1.232690	-0.533016	-0.519524
0.250000	1.271332	-0.005780	1.265552	-0.616285	-0.601622
0.178606	1.299977	-0.006129	1.293847	-0.689939	-0.674041
0.116978	1.338998	-0.006662	1.332336	-0.792915	-0.775120
0.066987	1.398211	-0.007654	1.390557	-0.954993	-0.933648
0.033134	1.492036	-0.009812	1.482224	-1.226171	-1.196989
0.007546	1.654753	-0.015487	1.639256	-1.738208	-1.687193
0.	1.222838	-0.025387	1.197451	-0.495333	-0.433890
0.007546	0.230617	^ .15110	0.245727	0.948816	0.939618
0.033134	0.677735	0.009398	0.687103	0.540715	0.527889
0.066987	0.847027	0.007264	0.854292	0.282545	0.270186
0.116978	0.931115	0.006319	0.937434	0.133025	0.121217
0.178606	0.982953	0.005850	0.988803	0.033803	0.022269
0.250000	1.018643	0.005575	1.024218	-0.037634	-0.049022
0.328990	1.035220	0.005338	1.040558	-0.071680	-0.082761
0.413176	1.029507	0.005071	1 036578	-0.059885	-0.070352
0.500000	1.019180	0.004772	1.023953	-0.038729	-0.048479
0.586824	1.005821	0.004421	1.010242	-0.011675	-0.020588
0.671010	0.991961	0.004020	0.995981	0.016053	0.008062
0.750000	0.978717	0.003565	0.982282	0.042112	0.035122
0.821394	0.967527	0.003062	0.970589	0.063891	0.057956
0.883022	0.956528	0.002544	0.959032	0.085055	0.080258
0.933013	0.942939	0.001906	0.944844	0.110867	0.107269
0.969846	0.924185	0.001268	0.925453	0.145882	0.143537
0.992404	0.886534	0.000656	0.887190	0.214058	0.212894
1.000000	0.	0.	0.	1.000000	1.000000

INTEGRATED CN= 0.425593
INTEGRATED CC= -0.030299
INTEGRATED CM(X)= 0.002425 C= ABT X=.25
INTEGRATED CM(Y)= -0.001200 C= ABT Y=0

AML PROBLEM 840-041.ARBITRARY AIRFOIL PRESSURE DISTRIBUTION
WITH EMPIRICAL CORRECTION FOR VISCOSITY

PRESSURE DISTRIBUTION

RAE-101-010

ALFA	CL	DELTA	SIN(ALFA)	LIFT SLOPE	ALFA,CL=0
4.090000	0.430129	0.003146	0.071323	0.959000	-0.

INTERMEDIATE VALUES

UPPER SURFACE

X	POTNL VELOC	VISC INCRM	VISC VELOC	POTNL P/Q	VISC P/Q
0.000076	1.372143	-0.025188	1.346954	-0.882775	-0.814285
0.000305	1.491405	-0.024563	1.466841	-1.224288	-1.131623
0.000685	1.578801	-0.023607	1.555194	-1.492614	-1.418629
0.001218	1.636931	-0.022440	1.614490	-1.679542	-1.606578
0.001903	1.670912	-0.021175	1.649737	-1.791948	-1.721832
0.002739	1.686517	-0.019899	1.666618	-1.844338	-1.777616
0.003727	1.688984	-0.018667	1.670317	-1.852667	-1.785959
0.004866	1.682542	-0.017513	1.665028	-1.830946	-1.772319
0.006156	1.670352	-0.016452	1.653900	-1.790074	-1.735384
0.011852	1.609742	-0.013469	1.596273	-1.591269	-1.548087
0.017037	1.565266	-0.011923	1.553343	-1.450059	-1.412874
0.023142	1.525772	-0.010735	1.515037	-1.327982	-1.295338

LOWER SURFACE

X	POTNL VELOC	VISC INCRM	VISC VELOC	POTNL P/Q	VISC P/Q
0.000076	1.050412	-0.025123	1.025289	-0.103366	-0.051217
0.000305	0.865489	-0.024437	0.841053	0.250928	0.292631
0.000685	0.679460	-0.023425	0.656035	0.538334	0.569618
0.001218	0.501721	-0.022211	0.479510	0.748276	0.770070
0.001903	0.338321	-0.020906	0.317415	0.885539	0.899248
0.002739	0.192062	-0.019597	0.172465	0.963112	0.970256
0.003727	0.063355	-0.018339	0.045015	0.995986	0.997974
0.004866	0.048822	0.017165	0.065987	0.997616	0.995646
0.006156	0.146171	0.016087	0.162258	0.978634	0.973672
0.011852	0.396978	0.013070	0.410048	0.842408	0.831860
0.017037	0.517400	0.011514	0.528914	0.732297	0.720250
0.023142	0.607684	0.010321	0.618006	0.630720	0.618069

Figure 6 – Typical Output from Computer, Pressure Distribution

velocity given by Equation [20]:

$$C(-)\cos\alpha + D(-)\sin\alpha + \Delta\alpha E(-) = 0$$

Usually two iterations are necessary to solve this equation.

Also, if the nose radius is desired, it may be found from

$$\rho_{LE} = 2\left[-\frac{dY}{d\varphi}(-)\right]^2$$

If the nose radius is known, this relation provides a check of the computed slope.

Two pages titled "Pressure Distribution" are printed (Figure 6) for each input angle. The first is the pressure distribution at the specified points and the second is the pressure distribution at the intermediate points near the nose. Constants printed out at the top of the page are for the input conditions. "Delta" stands for $\Delta\alpha$, calculated from Equation [18], and is given in radians. A measure of the accuracy of the input data is the smoothness of the curve $\frac{dY}{d\varphi}$ since small errors in the ordinates are magnified when taking the slope.

At the bottom of the page with the pressure distribution at the input points (Figure 6) are integrated values for:

$C_N = -1/2 \oint_0^{2\pi} C_p \sin\varphi\, d\varphi$ — The coefficient of force normal to the chordline, (positive upward)

$C_c = -\oint_0^{2\pi} C_p Y'(\varphi)\, d\varphi$ — The coefficient of force parallel to the chordline (positive in the positive x-direction)

$C_M\big|_{x=.25} = 1/2 \oint_0^{2\pi} C_p \sin\varphi\,(x-.25)\, d\varphi$ — Moment about the line x = 0.25 (clockwise positive)

$C_M\big|_{y=0} = -\oint_0^{2\pi} C_p\, Y\, Y'(\varphi)\, d\varphi$ — Moment about the line Y = 0 (clockwise positive)

The lift coefficient is given by $C_L = C_N \cos\alpha - C_c \sin\alpha$, and the moment coefficients about the point (0.25, 0) are given by $C_m(0.25,0) = C_m\big|_{x=0.25} + C_m\big|_{Y=0}$.

The integrals are evaluated with the trapezoidal rule at equal angular intervals. The numerically integrated values should be reasonably accurate, except C_c since there is not a smoothing factor (e.g., $\sin\omega$, Y) under the integral sign. In fact, the pressure program gives a nonzero chord force for foils at zero incidence. (Potential theory gives zero drag.)

In all cases considered so far, the integrated and set lift coefficients have agreed within 2 percent.

COMPARISON OF POTENTIAL THEORY WITH OTHER METHODS

Here, comparisons will be made with other methods for calculating two-dimensional pressure distributions in potential flow. Substituting Equation [6] into Equation [15], we find for the potential velocity on the profile

$$\frac{q}{U} = \frac{1}{\sqrt{\frac{\sin^2\varphi}{4} + Y'(\varphi)^2}} \Bigg| \cos\alpha \left[1/2 \sin\varphi - 1/2\pi \int_0^{2\pi} Y'(t) \left(\cot\frac{t-\varphi}{2} - \cot t/2 \right) dt \right] + \sin\alpha \left[\frac{1-\cos\varphi}{2} - Y'(\varphi) + Y'(0) \right] \Bigg| \qquad [31]$$

This is equivalent to the solution obtained by Moriya.[8,10]

Converting this expression to x dependence, we obtain

$$\frac{q}{U} = \frac{1}{\sqrt{1 + Y'(x)^2}} \left| \cos\alpha \left[1 + 1/2\pi \int_0^1 \frac{Y_U'(\xi) - Y_L'(\xi)}{x - \xi} \, d\xi \right. \right.$$

$$\left. \pm 1/2\pi \sqrt{\frac{1-x}{x}} \int_0^1 \sqrt{\frac{\xi}{1-\xi}} \, \frac{Y_U'(\xi) + Y_L'(\xi)}{x - \xi} \, d\xi \right]$$

$$\left. + \sin\alpha \left[\pm \sqrt{\frac{1-x}{x}} + Y'(x) - \frac{\left(Y'(x) \sqrt{1-x} \right)_1}{\sqrt{x(1-x)}} \right] \right| \qquad [32]$$

where $0 \leq x \leq 1$, and Y_U and Y_L are the upper and lower surface ordinates, respectively, measured from the nose-tail line, and primes denote differentiation with respect to the argument.

Riegels and Wittich[17] obtained this same equation by noting that linear airfoil theory, including the thickness correction term in sin α, gives a velocity on the chordline. They obtained the velocity on the profile from the linearized velocity $q(x,0)$ by equating integrands of two expressions for the circulation:

$$\Gamma = \oint q(x,Y)\, ds = \oint q(x,0)\, dx$$

$$\text{i.e.,} \qquad q(x,Y) \approx \frac{q(x,0)}{ds/dx} = \frac{q(x,0)}{\sqrt{1 + Y'(x)^2}}$$

since the singularities enclosed by both paths are the same. This neat trick can also be used to improve three-dimensional linear theory.[13, 14]

Equation [32] clearly shows the cross-coupling effects of thickness and camber in the velocity distribution. If the thickness and camber are added and subtracted to

obtain the ordinates, then the only coupling at zero incidence is the term $\sqrt{1 + Y'(x)^2}$ which is negligible except near the nose. Hence the NACA method of combining velocity increments computed separately for thickness and camber can be expected to be accurate everywhere except near the nose. Comparative calculations have shown that using the NACA tabulated velocity increments[15] is sufficiently accurate for most sections but that there is simply not enough data near the nose even for moderate incidence.

In References 13 and 14, Weber proposes a method of calculating two-dimensional pressure distributions which is based on other work of Riegels. Her expressions for $C(\varphi)$ (Equation [15]) is the same as ours, but for $D(\varphi)$ she obtains

$$D(\varphi) \equiv D(x) = \sqrt{\frac{1-x}{x}} \; \frac{1 + \frac{1}{\pi}\int_0^1 \left[Y_T'(\xi) - \frac{Y_T(\xi)}{2\xi(1-\xi)} \right] \frac{d\xi}{x-\xi}}{\sqrt{1 + Y'(x)^2}}$$

where $Y_T = 1/2\,(Y_U - Y_L)$.

This expression gives results which are closer to exact potential theory than does the method presented earlier in this paper. However the derivation is somewhat loose when camber is included and the method does not easily allow the insertion of the experimental lift while satisfying the Kutta condition.

The data tabulated in Reference 15 will be used to compare the approximate potential solution, Equation [32], with the exact solution for the more usual foils in use today. Theoretical velocity contributions for a large number of arbitrary thickness forms, calculated numerically from Theodorsen's exact method for potential flow, are tabulated there. Pressure distributions at zero angle of attack calculated by that

method and by the method of this report are compared for three foils--the NACA 16-009,* the NACA 0010, and the NACA 65A-006. As shown in Figures 7 and 8, the two methods are in close agreement for both the NACA 16-009 and the NACA 0010. However, for the 65 form (Figure 9) the method of this report predicts a small pressure peak near the nose. Plotting the ordinates at the angular variable $\theta = \arccos(2x - 1)$ instead of the usual x, we find a hump near the nose (Figure 10). This hump causes the pressure peak since fairing it out was found to give a smooth pressure curve. The numerical method of Hess and Smith[18] predicts a similar peak on this foil (see Figure 42 of Reference 18). They note the important point that experiments fail to show the peak. The experimental discrepancy is thought by the authors to be the result of inaccurate machining near the nose.

To explain the theoretical differences, note the discussion on page 3 of Reference 19 in connection with the design of the NACA 16 series:

> "The Theodorsen method as ordinarily used for calculating the pressure distributions about airfoils, was not sufficiently accurate near the leading edge for prediction of the local pressure gradients."

Because of this deficiency, Theodorsen's numerical evaluation of a nonlinear integral equation was not used for the design of the NACA 6 series foils, but was replaced by another numerical procedure employing equations similar to the interpolation functions

*The equations

$$Y_T = \tau \left[.98883\sqrt{x} - .23702\,x - .04398\,x^2 - .55762\,x^3\right], \quad 0 \leq x \leq .5$$

$$Y_T = \tau \left[.01 + 2.325\,(1-x) - 3.42\,(1-x)^2 + 1.46\,(1-x)^3\right], \quad .5 \leq x \leq 1$$

give a good fit to the tabulated ordinates for the NACA 16 form. The nondimensional nose radius is $0.4889\,\tau^2$, or 0.003960 for the original 9-percent thick foil.

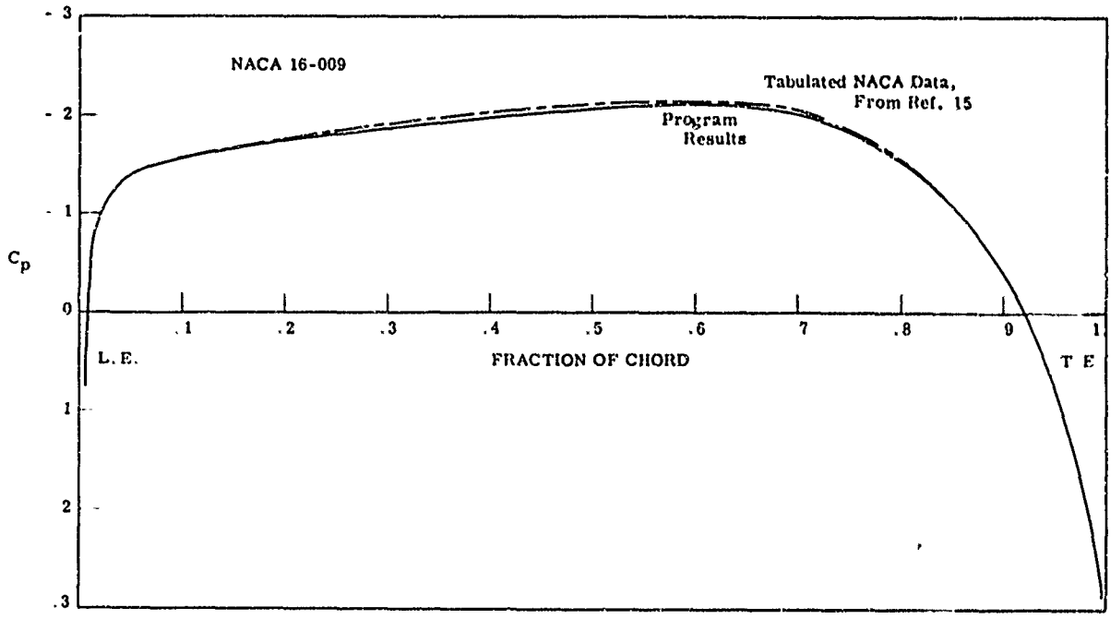

NACA 16 - 009

X	Y_T
.0	.0
.007598	.00759
.030154	.01481
.066987	.02157
.116978	.02781
178606	.03339
.25	.03813
.328090	.04181
.413176	.04418
.5	.045
.586824	.04408
.671010	.04111
.75	.03603
.821394	.02920
.883022	.02140
.933013	.01358
969846	.00693
.992404	.00247
1.0	.00090

Figure 7 – Comparison of Theoretical Pressure Distributions for NACA 16-009, Zero Incidence

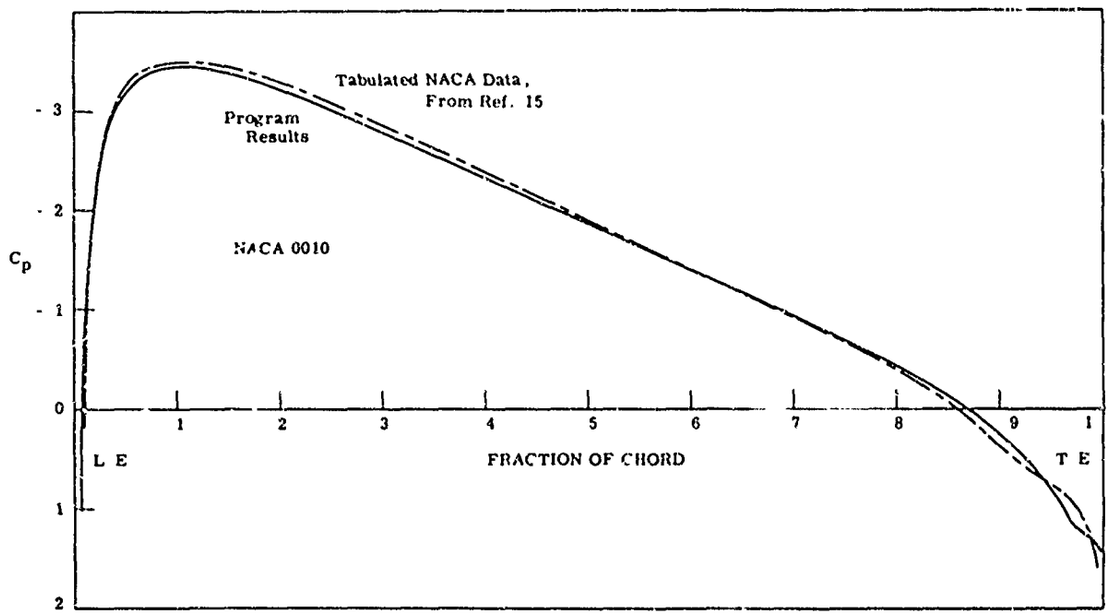

NACA - 0010

X	Y_T
.0	.0
.007596	.01245
.030154	.02372
.066987	.03345
.116976	.04122
.178606	.04664
.25	.04951
.328090	.04986
.413176	.04793
.5	.04412
.586824	.03892
.671610	.03283
.75	.02634
.821394	.01986
.883022	.01381
.933013	.00857
.969846	.00451
.992404	.00193
1.0	.00105

Figure 8 – Comparison of Theoretical Pressure Distributions for NACA 0010, Zero Incidence

for the ordinates (Equations [23] and [24]) used in this report.[19, 15] For these foils, it is believed that the complicated behavior of the "design parameters" near the nose (see Figure 4 on page 9 of Reference 19) is not adequately represented by such a finite term approximation for the Fourier series unless a large number of terms is used. Note, in contrast, the smoothness of the curves Y (φ); see, e.g., Figure 10. Accurate integration of an irregular curve would depend upon the number of points taken. Theodorsen[6] recommended five equal divisions between 0 and π with his method. Reference 15 recommends 40 with the improved method, surely more than enough. No indication of the number used in the design process is given in Reference 19, but it is believed to have been insufficient.

So far, comparisons have been made only for thickness distributions at zero angle of attack. For cambered foils at an angle of attack, a potential theory ($\Delta\alpha = 0$) comparison can be made or $\Delta\alpha$ may be adjusted to give the same lift. Both comparisons are shown in Figure 11 for the 4412 at $\alpha = 6.4$ degrees. (Pinkerton[4] gives the potential lift, computed numerically from exact theory, as $C_L = 6.915 \sin(\alpha - \alpha_o)$, $\alpha_o = -0.0706$ radians.) It is easily seen that the computed pressure distribution with the exact lift ($C_L = 1.254$) is not in agreement with the results of the exact potential theory. It should be noted that the results of the exact theory were taken from the small figure on page 62 of Reference 15. Even allowing for errors in the transfer of data, the agreement is only fair at the same lifts. Moreover, the computed minimum pressure is about 10 percent lower than the "exact," which follows the trend in Appendix A. Integration of the curves in Figure 11 gives

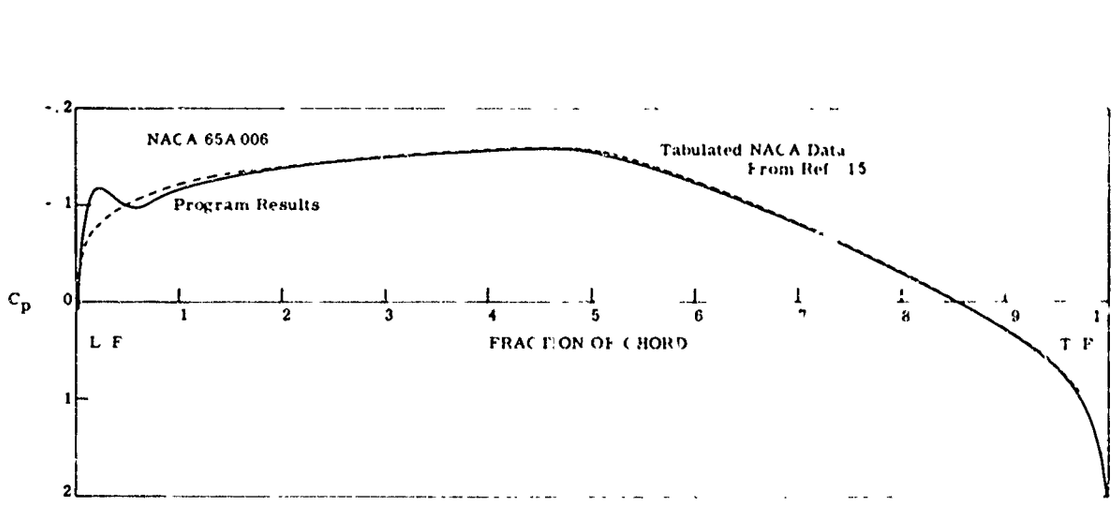

NACA 65A 006

X	Y_T
0	0
007596	00566
030154	01061
066987	01567
116978	01962
178606	02363
25	02687
328990	02908
413176	03000
5	02925
586824	02657
671010	02252
75	01775
821394	01287
883622	00848
933013	00491
969846	00228
992404	00067
1	00013

Figure 9 – Comparison of Theoretical Pressure Distributions for NACA 65A006, Zero Incidence

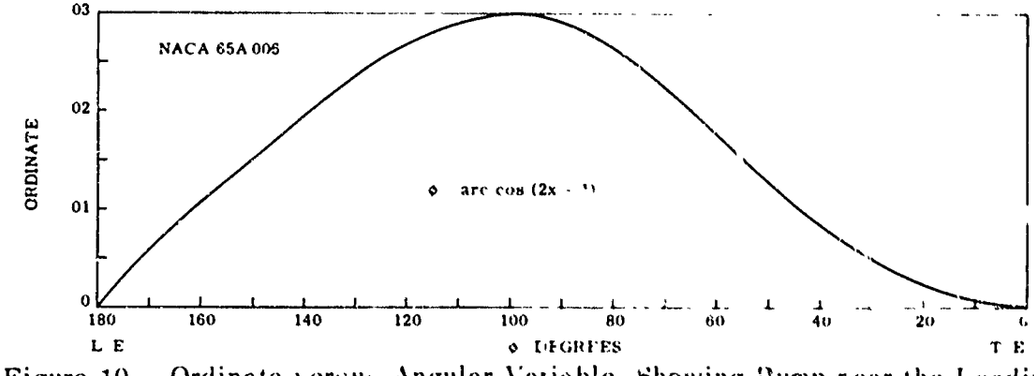

Figure 10 – Ordinate versus Angular Variable, Showing Bump near the Leading Edge, NACA 65A006

C_L = 1.274 for the "exact" pressure distribution and C_L = 1.242 for the approximate case ($\Delta\alpha \neq 0$), compared to the set C_l of 1.254. The difference between the set and integrated value for the pressure program (approximately 1 percent) is thought to be caused by the approximations in the theory and possibly by inaccuracies in the numerical method. The disagreement between the "exact" results and the integrated value (approximately 4 percent) is obviously caused in part by the small size of the original curve of exact pressure from which the data were taken. Some of the discrepancy could also be a result of Pinkerton's use of approximate expressions for ϵ and ϵ_o. That these are approximations is apparent if one compares the expressions on page 13 of Reference 4 with those in Reference 6 and in the section on empirical modification given in the present paper.

COMPARISON WITH EXPERIMENTAL RESULTS

COMPARISON WITH MEASURED PRESSURE DISTRIBUTIONS

There are few measured pressure distributions tabulated at a sufficient number of points to accurately define the pressure curve near the nose. The most comprehensive tests are those of Pinkerton[7] on the NACA 4412 section. Unhappily, Pinkerton's measurements are actually for three-dimensional flow over a rectangular foil with a 30-inch span and a 5-inch chord. The equivalent two-dimensional flow is found by subtracting the theoretically calculated induced angle of attack from the geometric angle of incidence. Nevertheless, these tests are often used in two-dimensional comparisons because of a general lack of experimental data, and for that reason, we do so also.

Comparison of pressure distributions on the NACA 4412 section at an equivalent two-dimensional flow angle of 6.4 degrees (geometric incidence of 8 degrees) is shown in Figure 12. Agreement on the upper surface is excellent, but the lower surface shows slight differences. As expected, there is disagreement near the trailing edge caused by the thickening boundary layer. Also shown in Figure 12 is the pressure distribution computed from ordinates interpolated (in the pressure program) from the tabulated measured[4] offsets of the foil. Some of the humps and hollows in the measured pressure distribution are better predicted, but a new predicted hump is also obtained at quarter chord. (The measured nondimensional ordinate at this point is 0.0012 greater than the computed value.) Essentially though, the pressure distribution is the same as for the mathematical ordinates.

Reference 3 contains one of the few tabulated sets of measured two-dimensional pressure distributions with a sufficient number of experimental points near the nose. The model tested was a symmetric RAE 101 section with a 30-inch chord and 10-percent thickness ratio. The large model (surfaces were accurate to $\pm$ 0.0003 c) and accurately measured angle of incidence (to the nearest 0.01 degree) makes these tests valuable for comparative purposes.

Two Reynolds numbers were considered in the experiments. For comparison, we have selected the lower ($R_e = 1.6 \times 10^6$) since it corresponds to a lower Mach number (U = 100 ft/sec). (It is not completely clear whether or not compressibility corrections were applied to the data.) Measured and predicted pressure distributions are shown in Figures 13, 14, and 15 for three angles of attack: 0, 2.05, and 4.09

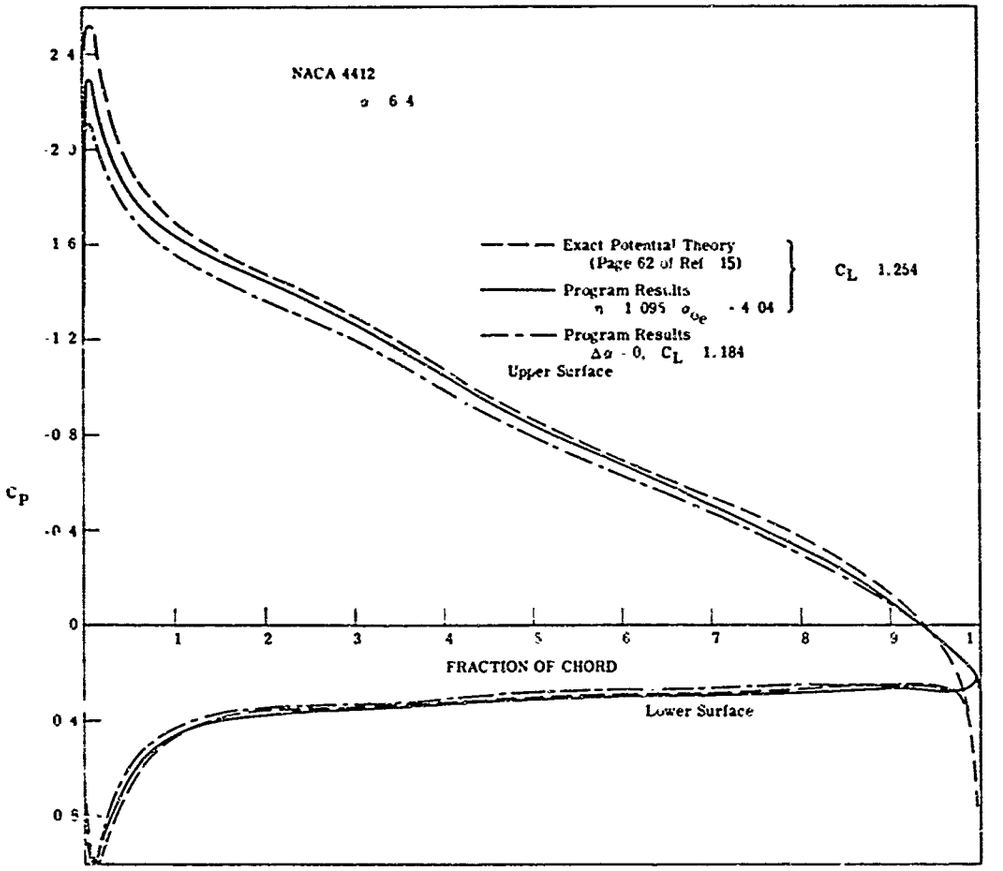

Figure 11 – Comparison of Theoretical Pressure Distributions for NACA 4412, = 6.4 Degrees

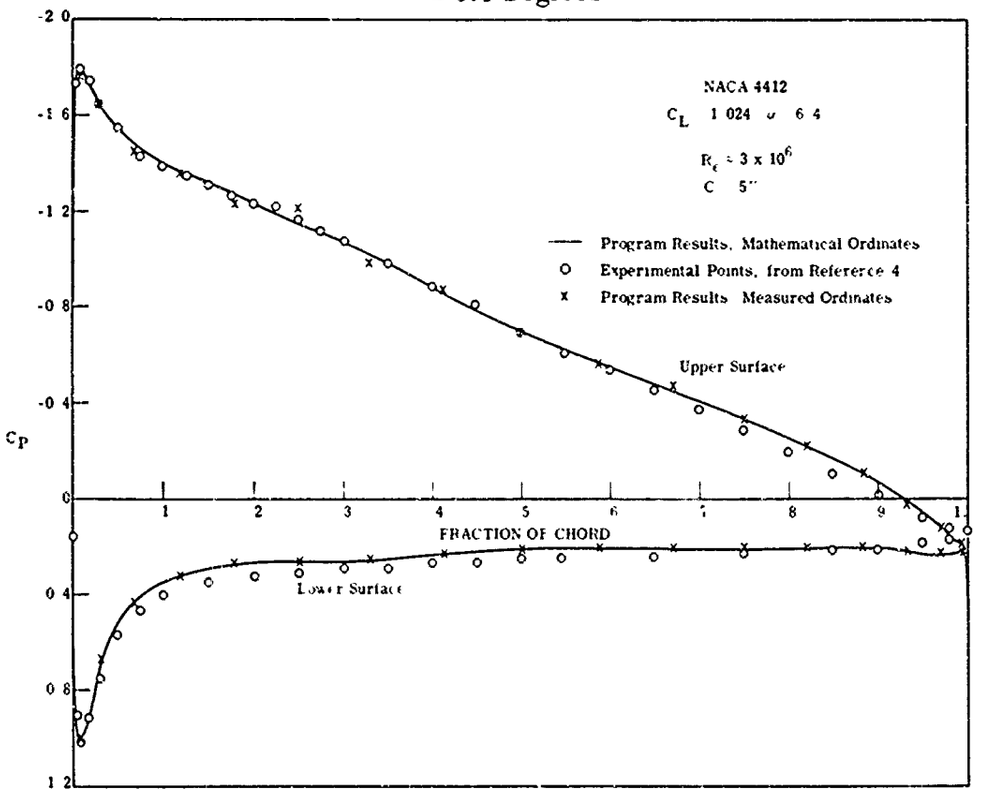

Figure 12 – Measured and Predicted Pressures on the NACA 4412, C_L = 1.021, α = 6.4 Degrees

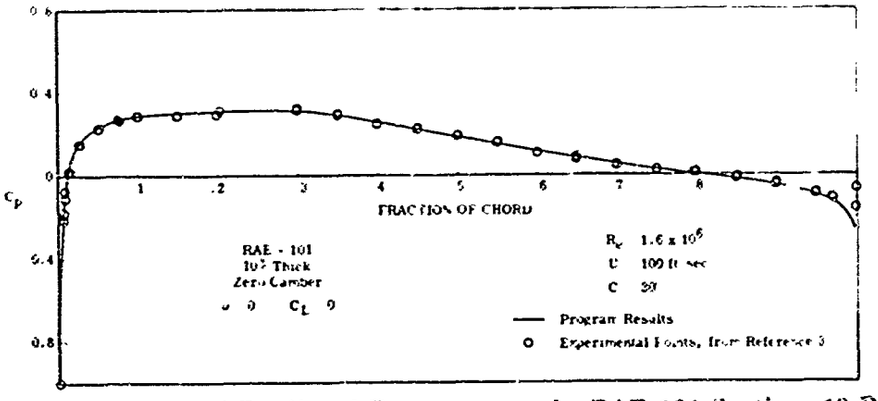

Figure 13 – Measured and Predicted Pressures on the RAE 101 Section, 10-Percent Thick. $C_L = 0$, $\alpha = 0$

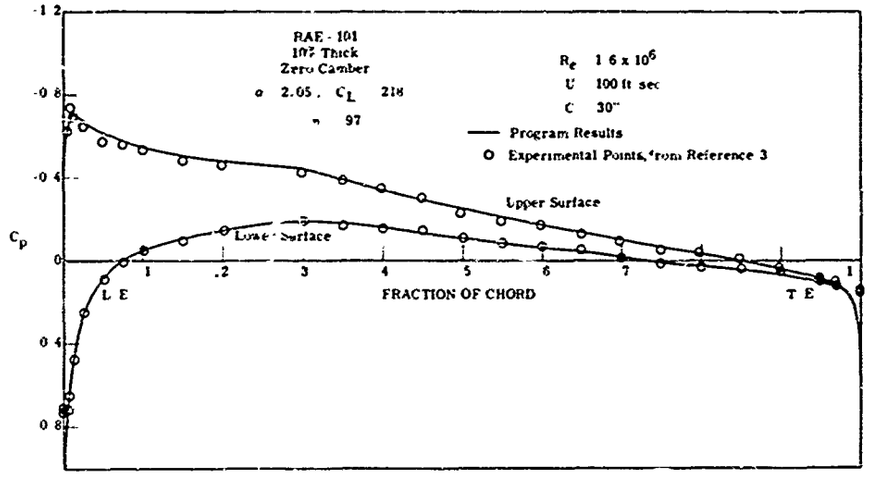

Figure 14 – Measured and Predicted Pressures on the RAE 101 Section, 10-Percent Thick, $C_L = 0.218$, $\alpha = 2.05$ Degrees

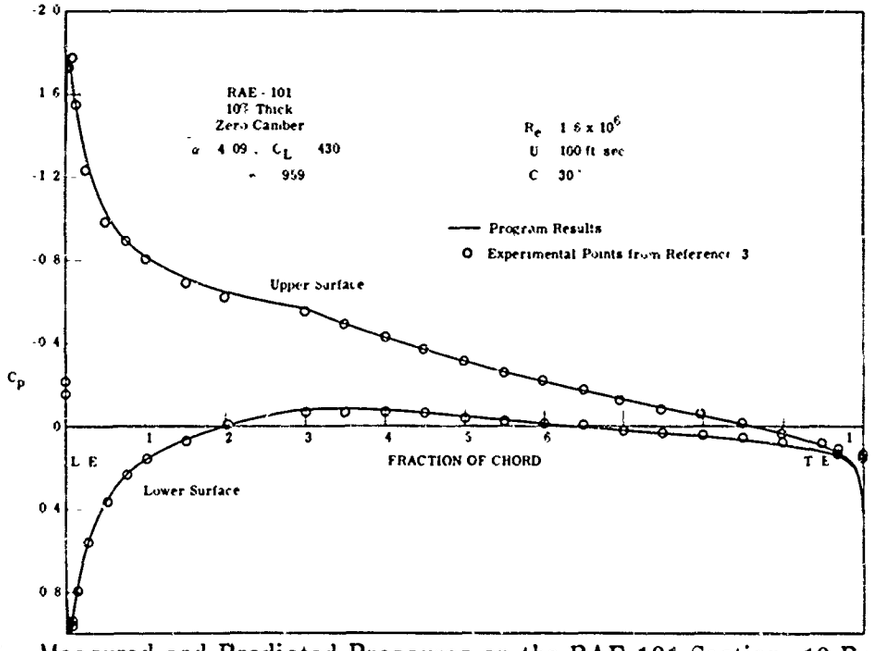

Figure 15 – Measured and Predicted Pressures on the RAE 101 Section, 10-Percent Thick, $C_L = 0.430$, $\alpha = 4.09$ Degrees

degrees. Agreement is excellent except at the trailing edge. This deviation is again due to the rapid thickening of the boundary layer at the trailing edge.

COMPARISON WITH MEASURED CAVITATION INCEPTION

Although measured pressure distributions are hard to find, incipient cavitation tests have been conducted in several laboratories. With the classical assumptions that cavitation starts when the local pressure falls to the vapor pressure of the flowing liquid, cavitation inception may be predicted from the pressure distribution since the cavitation index $\sigma_i = \frac{p_\infty - p_v}{1/2\rho U^2}$ is equal to minus the minimum pressure coefficient $-C_{P_{min}} = \frac{p_\infty - p_{min}}{1/2\rho U^2}$. It is important to note that unsteady effects are not considered when computing the minimum pressure. That is, the testing is actually done for either varying P_∞[21] or α[22] whereas the predictions are for fixed flow conditions. This means that there is some doubt that the predicted miminum coincides with the actual test minimum. Assuming that they are equal is the usual "quasi-steady" approach, generally the only reasonable basis of solution. For the (assumed) slow variations in flow conditions here, it is reasonable to expect they would be equal.

Cavitation inception data from two different laboratories will be considered: (1) tests by the California Institute of Technology (CIT)[21] on the NACA 4412 section for various Reynolds numbers and (2) tests by Vosper Limited[20] on elliptic-parabolic sections of various thickness and camber ratios (NACA a = 1 camberline) at constant Reynolds number (R_e = 1x 10).

Measured values[21] of σ_i for (visual) inception and disappearance of cavitation at two different Reynolds numbers are compared with measured[20] values of $-C_{P_{min}}$

for the NACA 4412 in Figures 16a and 16b. Predicted minimum pressures were computed for values of η and α_{o_e} interpolated from subcavitating tests of the foil used in the inception tests.

The good agreement of predicted and measured $-C_{P_{min}}$ is surprising since the angles of zero lift and lift-curve slopes are not the same in the various tests. Also, for negative angles of attack, the measured pressure distribution was not taken at a sufficient number of points to ensure obtaining the minimum pressure.

Cavitation prediction from computed minimum pressure is not in such good agreement (the prediction is conservative) although agreement improves with increasing test free-stream velocity. Some of the discrepancy may be attributed to nonsteady effects (resulting in a poor prediction of the minimum pressure) although, as already discussed, such effects should be small. Again the fault seems to be with the assumption that cavitation begins when the local pressure falls to the vapor pressure.* Perhaps equally important in accounting for the inaccurate prediction is the small size of the model (3-inch chord). For such a small model, slight machining errors could result in large changes from the computed pressure distribution. It would thus be of considerable interest to have measured ordinates rather than ordinates for only the mathematical foil.

Machining should be most inaccurate for the rapidly changing geometry of the nose, and at negative angles of attack, the minimum pressure is close to the nose.

*This has been known for a considerable time although it is generally assumed that for "engineering problems," conditions are such that the assumption is adequate. (See References 23 and 24.)

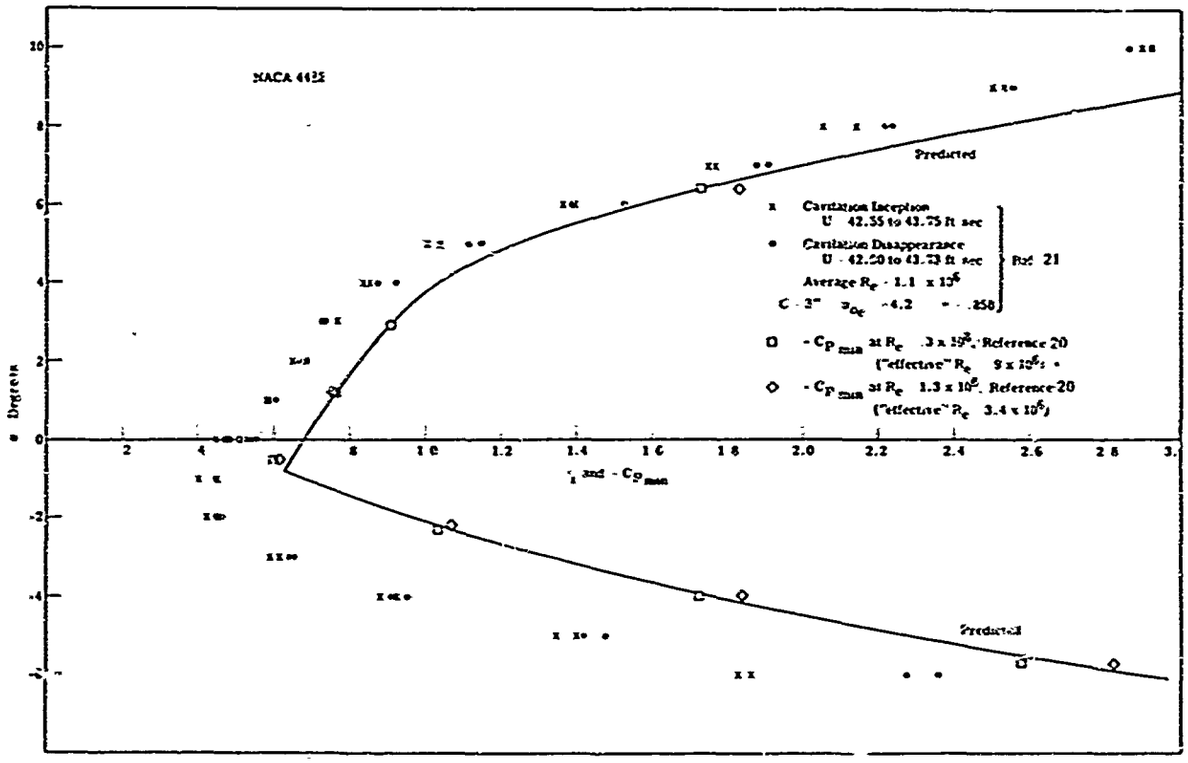

Figure 16a — Comparison at $R_e = 1.1 \times 10^6$

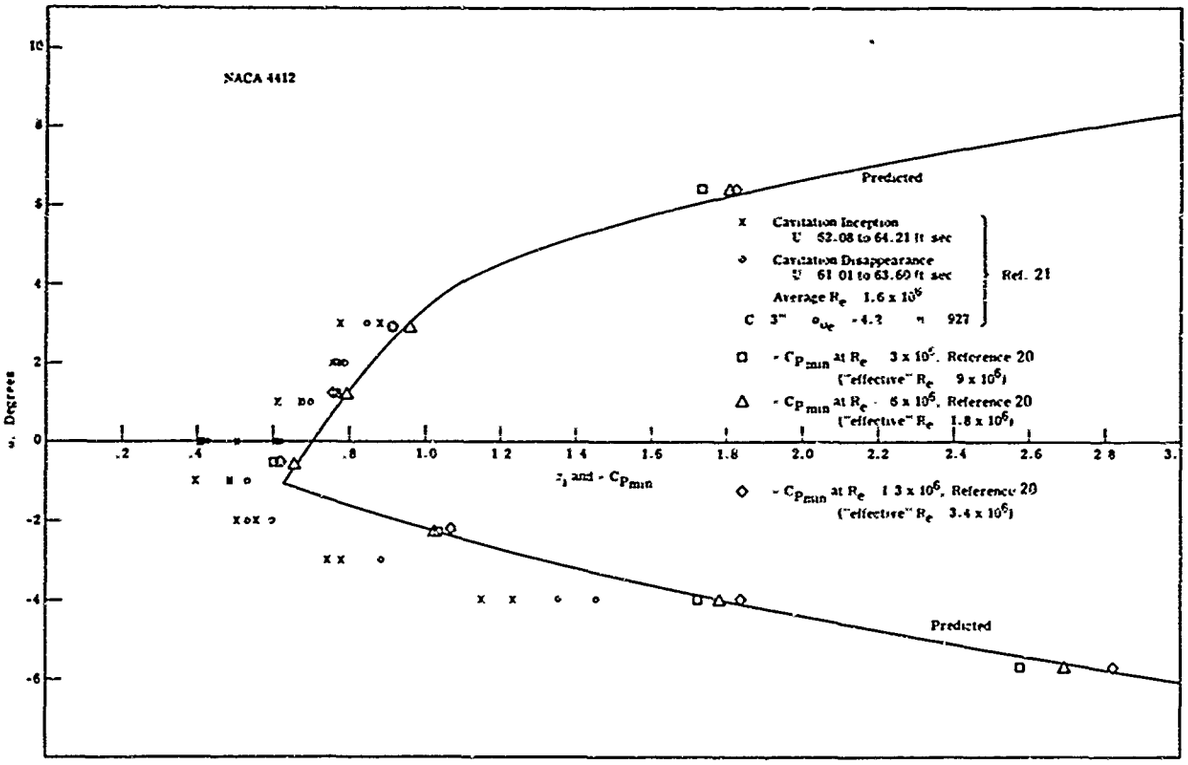

Figure 16b — Comparison at $R_e = 1.6 \times 10^6$

Figure 16 — Comparison of Incipient Cavitation Number and Minimum Pressure Coefficient, NACA 4412

It is possible, then, that machining inaccuracies also contribute to the large differences at negative incidence.

Since the incipient cavitation number for two-dimensional hydrofoils increases with increasing free-stream velocity and since, in "certain instances," increasing the body size also increases the incipient cavitation number,[25] it is imperative that, with our present lack of knowledge of the proper scaling laws, laboratory testing should be done for environments approaching full-scale conditions if meaningful data are to be taken. A better alternative is to develop realistic scaling laws so that models of small size may be tested at low Reynolds numbers.

The cambered 9-percent thick foil was selected for comparison with the Vosper test data. In these tests, only (visual) cavitation disappearance was recorded. Experimental and predicted values are shown in Figure 17. Figure 17a gives the raw data points and Figure 17b the faired data corrected (by Vosper) for tunnel interference. The raw data are included to show the experimental scatter. In both cases, the prediction is based on the experimental lift-curve slope corrected for tunnel interference. The raw data show that the agreement for angles greater than zero is generally good except for the one point at 1/2 degree. For negative angles of attack, the prediction is again too conservative.

Although the model chord was relatively large (8 inches) in these tests, the machining was accurate to only ± 0.005 inch[22] or ± 0.0006c. From actual numerical test cases run using the pressure program, *random* differences of this size in the ordinates could account for the unusual result that $\alpha_i >- C_{p_{min}}$ near zero angle

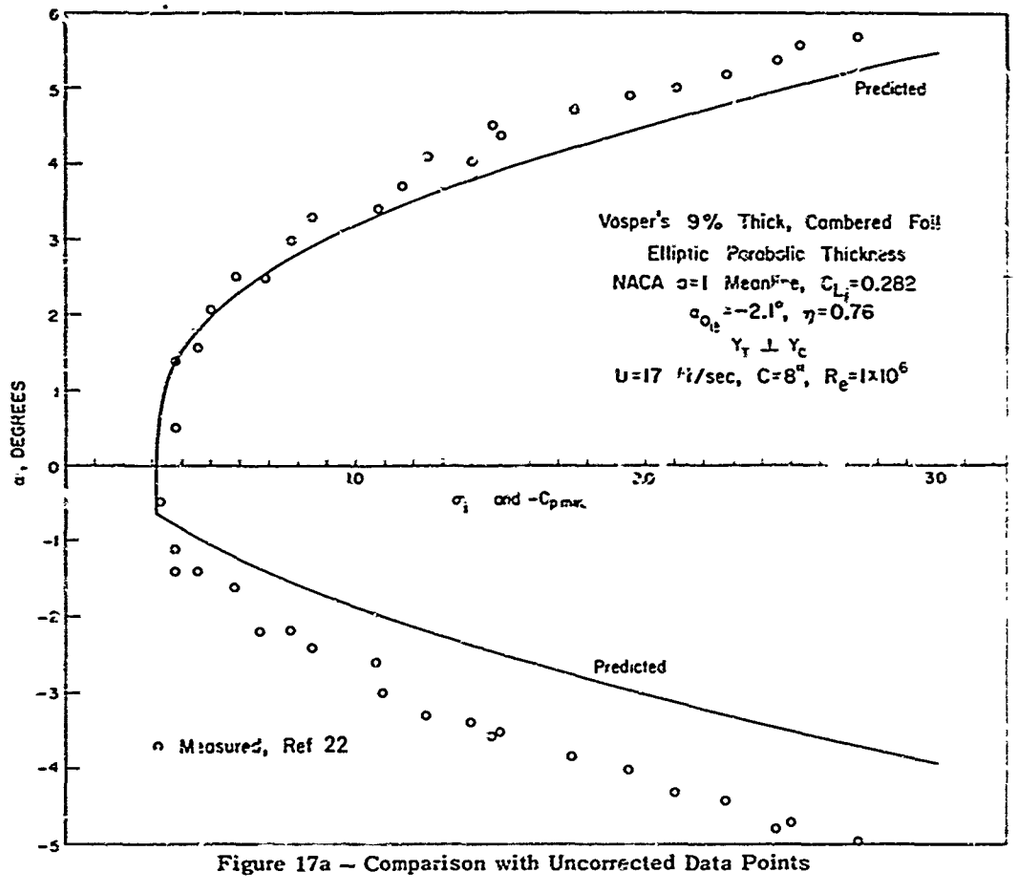

Figure 17a – Comparison with Uncorrected Data Points

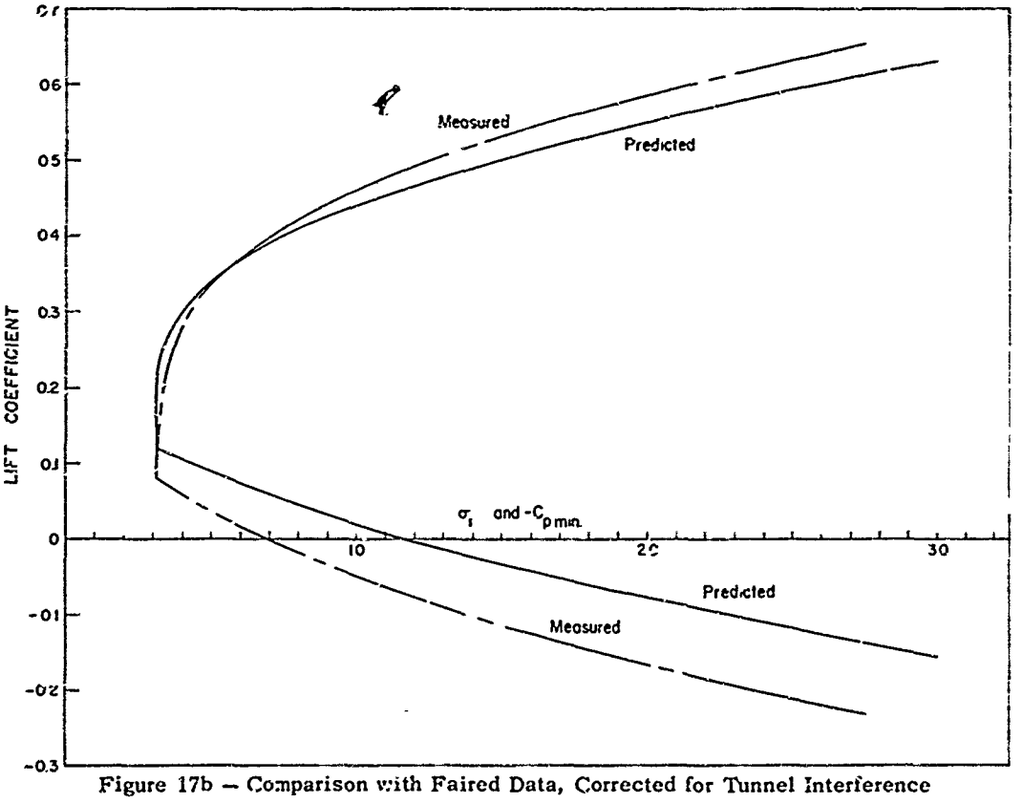

Figure 17b – Comparison with Faired Data, Corrected for Tunnel Interference

Figure 17 – Comparison of Incipient Cavitation Number and Minimum Pressure Coefficient, Elliptic-Parabolic Section, NACA a = 1.0 Meanline

of attack. (However, $\sigma_i > -C_{P_{min}}$ at small incidences was also found for other foils tested by Vosper. It is interesting to note that the air content during these tests was only 50 percent of saturation[22] whereas air content for the CIT tests was about 85 percent of saturation.[21])

Although measured ordinates would be useful in determining more precisely the differences between σ_i and $-C_{P_{min}}$, the differences are too great to be attributed solely to inaccurate machining. Most of the differences seem a result of assuming that cavitation occurs when the local pressure falls to the vapor pressure.

SUMMARY AND CONCLUSIONS

A numerical method for calculating the two-dimensional pressure distribution on arbitrary profiles with arbitrary lift has been explained. The development is based on an empirically modified, approximate, conformal transformation of the circle and is limited to flow conditions before stall. In all cases considered so far, the numerical approximate method gives integrated lift coefficients that differ by less than 2 percent from the assigned value.

For the examples tested, when the pressure distribution about a foil at a given incidence is computed with the appropriate lift, agreement is good with both exact potential theory and experimental results. Comparisons with measured pressure distributions show considerable disagreement near the trailing edge caused by the thickening boundary layer. The assumed empirical modification introduced in the potential theory cannot adequately represent the flow conditions near the trailing edge since it assumes a stagnation point there in contrast with the experimental result of almost free-stream pressure.

Although predicted pressure distributions agree well with measurement, comparisons of the minimum pressure coefficient and the incipient cavitation index show differences. In the example considered, the differences decrease with increasing test Reynolds number (i.e., free-stream velocity). Also, cavitation prediction on the upper surface is better than on the lower and is generally conservative on both. Some of the discrepancy may be explained by machining inaccuracies, especially near the nose. Hence, it would be of interest to have measured ordinates to use in the pressure program when making comparisons with the test results. If we assume that nonsteady effects in the testing were small, most of the differences seem a result of cavitation not occuring when the minimum pressure is equal to the vapor pressure. This points out the need for a better scaling law if laboratory data are to be useful in predicting full-scale results.

This investigation has called attention to two areas of deficiency in experimental results. First, there is a lack of pressure distributions on two-dimensional cambered foils. Second, cavitation inception tests have not been carried to the point of constant σ_i for increasing Reynolds number. Further investigation in both of these areas would be valuable to further confirm the calculation method of this paper.

ACKNOWLEDGMENTS

Special thanks are due Professor Geoffrey Ludford of Cornell University for his helpful suggestions, in particular, for catching inconsistencies in a previous development of the empirical modification.

APPENDIX A

EXAMPLES OF EXACT CONFORMAL TRANSFORMATION

If specific numbers are substituted for the transformation coefficients in Equations [2] and [3], we will obtain foil shapes from exact theory which can be used to check the approximate method where x has been approximated by Equation [4].

SYMMETRICAL FOILS

Consider first symmetrical shapes. These forms will be generated if all B_n are zero. For our purposes, sufficient generality is obtained by setting all A_n, $n > 2$, to zero. Then we have

$$x = A_o + (A_{-1} + A_1) \cos\varphi + A_2 \cos 2\varphi$$

$$Y = (A_{-1} - A_1) \sin\varphi - A_2 \sin 2\varphi$$

Letting $Y = \epsilon (\sin\varphi - \delta \sin 2\varphi)$ and requiring x to lie between 0 and 1, we obtain

$$x = 1/2 (1 + \cos\varphi) + \epsilon\delta \{\cos 2\varphi - 1)$$

From Equation [14], the exact velocity is obtained:

$$\frac{q}{U} = \frac{1/2 + \epsilon}{\sqrt{\left(\frac{dx}{d\varphi}\right)^2 + \left(\frac{dY}{d\varphi}\right)^2}} \quad [\sin\varphi \cos\alpha + (1 - \cos\varphi) \sin\alpha]$$

Also, from Equation [12] the lift coefficient is

$$C_L = 2\pi (1 + 2\epsilon) \sin\alpha$$

First, consider the case $\delta = 0$, then

$$Y = \epsilon \sin$$

$$x = 1/2\,(1 + \cos\varphi)$$

which is the ellipse of thickness ratio $\tau = 2\epsilon$.

The velocity and lift coefficient are

$$\frac{q}{U} = (1 + \tau)\ \frac{\sin\varphi\cos\alpha + (1 - \cos\varphi)\sin\alpha}{\sqrt{\sin^2\varphi + \tau^2\cos^2\varphi}}$$

$$C_L = 2\pi\,(1 + \tau)\sin\alpha$$

(Note that this includes the special case of the flat plate, $\tau = 0$.)

Since x is precisely the form of the approximation, the velocity from the approximate method is also exact.

For the case of nonzero ϵ and δ, we can find φ in terms of x:

$$\varphi = \arccos \frac{\sqrt{1/4 - 8\,\delta\epsilon\,(1/2 - 2\,\epsilon\,\delta - x)} - 1/2}{4\,\delta\epsilon}$$

and obtain φ values which give x, Y, and q/U at the x values used in the numerical method. This has been done for four cases:

$$\delta = 1/2 \begin{cases} \tau = 0.2 \\ \tau = 0.1 \end{cases}$$

$$\delta = 1/4 \begin{cases} \tau = 0.2 \\ \tau = 0.1 \end{cases}$$

For $\delta = 1/2$, the foil has a cusped tail similar to the Joukowski foil. Maximum Y value occurs at $\varphi = 120$ degrees, from which $\epsilon = \dfrac{2\tau}{3\sqrt{3}}$. A comparison of exact and approximate values is given in Part (A) of the following table.

TABLE A-1

Comparison of Exact and Approximate Velocity Distribution for Two Foils

A) For the Foil:
$$\begin{cases} x = \frac{1}{2}(1 + \cos\varphi) + \frac{\tau}{3\sqrt{3}}(\cos 2\varphi - 1) \\ Y = \frac{2\tau}{3\sqrt{3}}(\sin\varphi - \frac{1}{2}\sin 2\varphi) \end{cases}$$

x	$\tau = .20$					$\tau = .10$				
	Y_T	C_{exact}	C_{approx}	D_{exact}	D_{approx}	Y_T	C_{exact}	C_{approx}	D_{exact}	D_{approx}
0	0	0	0	7.4952	6.4036	0	0	0	13.9904	12.9480
.007596	.031655	.7370	.7388	7.0136	5.9965	.014381	.9340	.9343	9.8212	9.0912
.030154	.059631	1.2296	1.2325	5.8179	4.9847	.027447	1.1659	1.1662	6.0849	5.6346
.066987	.081097	1.4283	1.4316	4.4618	3.8352	.038080	1.2116	1.2119	4.1636	3.8577
.116978	.094556	1.4422	1.4454	3.3303	2.8741	.045505	1.2072	1.2075	3.0565	2.8341
.178606	.099855	1.3799	1.3828	2.4984	2.1657	.049373	1.1846	1.1849	2.3431	2.1746
.25	.097881	1.2979	1.3004	1.9067	1.6603	.049755	1.1547	1.1549	1.8465	1.7154
.328990	.090159	1.2182	1.2204	1.4824	1.2965	.047083	1.1225	1.1228	1.4816	1.3779
.413176	.078485	1.1479	1.1499	1.1708	1.0282	.042038	1.0908	1.0910	1.2027	1.1197
.5	.064652	1.0882	1.0900	.9351	.8244	.035440	1.0609	1.0612	.9826	.9157
.586824	.050267	1.0386	1.0402	.7516	.6649	.028131	1.0339	1.0341	.8043	.7502
.671010	.036642	.9977	.9992	.6045	.5364	.020881	1.0099	1.0101	.6562	.6127
.75	.024738	.9645	.9659	.4832	.4299	.014317	.9893	.9894	.5304	.4956
.821394	.015149	.9379	.9392	.3804	.3392	.008881	.9719	.9721	.4212	.3939
.883022	.008111	.9171	.9184	.2909	.2598	.004805	.9579	.9581	.3242	.3033
.933013	.003540	.9016	.9028	.2108	.1886	.002114	.9471	.9472	.2361	.2210
.969846	.001074	.8908	.8919	.1372	.1228	.000645	.9394	.9396	.1542	.1443
.992404	.000136	.8844	.8855	.0676	.0606	.000082	.9348	.9350	.0761	.0713
1.0	0	0	0	0	0	0	0	0	0	0

B) For the Foil:
$$\begin{cases} x = \frac{1}{2}(1 + \cos\varphi) + \frac{\epsilon}{4}(\cos 2\varphi - 1) \\ Y = \epsilon(\sin\varphi - \frac{1}{4}\sin 2\varphi) \end{cases} \qquad \epsilon = .45417\,\tau$$

x	$\tau = .20$					$\tau = .10$				
	Y_T	C_{exact}	C_{approx}	D_{exact}	D_{approx}	Y_T	C_{exact}	C_{approx}	D_{exact}	D_{approx}
0	0	0	0	8.6728	7.9168	0	0	0	16.0122	15.3005
.007596	.025944	.7397	.7403	7.6502	6.9847	.012328	.9377	.9378	10.2197	9.7659
.030154	.049890	1.1375	1.1384	5.8403	5.3350	.023823	1.1206	1.1207	6.0605	5.7921
.066987	.070132	1.2895	1.2904	4.3603	3.9865	.033746	1.1585	1.1586	4.1239	3.9420
.116978	.085472	1.3270	1.3280	3.3070	3.0269	.041532	1.1621	1.1622	3.0462	2.9125
.178606	.095321	1.3143	1.3152	2.5600	2.3461	.046838	1.1532	1.1534	2.3602	2.2572
.25	.099687	1.2803	1.2812	2.0171	1.8513	.049562	1.1387	1.1388	1.8827	1.8012
.328990	.099066	1.2388	1.2397	1.6117	1.4813	.049827	1.1214	1.1215	1.5294	1.4637
.413176	.094293	1.1964	1.1972	1.3008	1.1973	.047942	1.1032	1.1033	1.2560	1.2024
.5	.086389	1.1563	1.1571	1.0565	.9738	.044342	1.0850	1.0851	1.0369	.9931
.586824	.076410	1.1201	1.1208	.8598	.7936	.039526	1.0678	1.0678	.8565	.8205
.671010	.065341	1.0881	1.0888	.6979	.6449	.033997	1.0518	1.0519	.7043	.6750
.75	.054009	1.0605	1.0611	.5615	.5194	.028205	1.0375	1.0375	.5730	.5493
.821394	.043034	1.0369	1.0375	.4438	.4109	.022512	1.0249	1.0250	.4573	.4385
.883022	.032809	1.0166	1.0171	.3399	.3149	.017162	1.0141	1.0142	.3533	.3388
.933013	.023505	.9976	.9982	.2457	.2278	.012279	1.0047	1.0048	.2577	.2472
.969846	.015089	.9733	.9739	.1578	.1464	.007867	.9948	.9949	.1679	.1611
.992404	.007356	.8984	.8988	.0723	.0670	.003830	.9695	.9696	.0812	.0779
1.0	0	0	0	0	0	0	0	0	0	0

For $\delta = 1/4$, the trailing edge is rounded and the general foil shape is similar to conventional foils. The maximum value of Y occurs at $\varphi = (\pi - \arccos \frac{\sqrt{3} - 1}{2})$, for which $\epsilon = 0.45417\,\tau$. A comparison with the approximate solution is given in Part (B) of the table.

These examples show negligible differences in the C (φ) component of velocity for the 10-percent thick foils. For the 20-percent thickness forms, the differences are larger but still slight. It is interesting to note that the approximate velocity is greater than the exact in this case. The D(φ) component of velocity shows large differences, but the approximate velocity is lower than the exact in this case, which is the trend indicated by viscous effects. Also this is the component of velocity which is multiplied by $\sin\alpha$ so that its contribution to the total velocity is small in the normal incidence range.

In general, these comparisons indicated that there are larger errors in the approximate computations for foils which show large departures from an ellipse. Most foils in use today have their maximum thickness near midchord and do not have cusped tails; both of these properties contribute to accurate calculations.

CAMBERED FOILS

For foils with camber, we consider terms in Equation [2] and [3] to the second harmonic, i.e.,

$$x = A_o + (A_{-1} + A_1)\cos\varphi + (B_1 - B_{-1})\sin\varphi + A_2\cos 2\varphi + B_2\sin 2\varphi$$

$$Y = B_o + (A_{-1} - A_1)\sin\varphi + (B_{-1} + B_1)\cos\varphi - A_2\sin 2\varphi + B_2\cos 2\varphi$$

We take

$$Y = \epsilon (\sin\varphi - \delta \sin 2\varphi) + \frac{f}{2} (1 - \cos 2\varphi) + \gamma (1 - \cos\varphi)$$

and set $\left.\frac{dx}{d\varphi}\right|_{\varphi = 0} = 0$, $x(0) = 1$, $x(\pi) = 0$ to obtain

$$x = 1/2 (1 + \cos\varphi) + \epsilon \delta (\cos 2\varphi - 1) + f \sin\varphi - \frac{f}{2} \sin 2\varphi$$

Unfortunately,* these foils do not have $\frac{dx}{d\varphi} = 0$ at the leading edge which means there is some overhang there. The constant γ is included to raise the nose to lie close to the x axis. The velocity distribution on these foils is

$$\frac{q}{U} = \frac{\left| \cos\alpha [(1/2 + \epsilon) \sin\varphi + (f + \gamma)(1 - \cos\varphi)] + \sin\alpha [(1/2 + \epsilon)(1 - \cos\varphi) - (f + \gamma) \sin\varphi] \right|}{\sqrt{\frac{dx^2}{d\varphi} + \frac{dy^2}{d\varphi}}}$$

where $\frac{dx}{d\varphi} = - 1/2 \sin\varphi + f \cos\varphi - 2 \epsilon\delta \sin 2\varphi - f \cos 2\varphi$

$$\frac{dy}{d\varphi} = \epsilon (\cos\varphi - 2\delta \cos 2\varphi) + \gamma \sin\varphi + f \sin 2\varphi$$

The lift coefficient is $C_L = 2\pi \frac{1 + 2\epsilon}{C} \sqrt{1 + \left[\frac{2(f + \gamma)}{1 + 2\epsilon}\right]^2} \sin(\alpha - \varkappa)$,

$\varkappa = -\arctan \frac{2(f + \gamma)}{1 + 2\epsilon}$.

The complexity of the $x(\varphi)$ term does not permit easy inversion to obtain $\varphi = \varphi(x)$. Instead, we simply calculated x, Y, and q/U at many φ values and put

*Nor do these expressions permit us to put $\epsilon = 0$ and obtain simply a camberline shape since the x relation would then give a curve which crosses itself and hence is meaningless.

the (x, Y) relation into the arbitrary input section of the pressure program. Since we were unable to calculate the exact velocity at the points of the numerical method, the comparisons must be made graphically.

The thickness portion of the foil was taken as $Y_T = \frac{2\tau}{3\sqrt{3}} (\sin\omega - 1/2 \sin 2\omega)$ with $\tau = 0.10$. The constants f and γ were first taken as 0.03 and 0.01, respectively, which gives a camber ratio of about 0.0369 and then f and γ were taken as 0.015 and 0.0075 which gives a camber ratio of about 0.0185. The foil shapes--rotated and shrunk to put the nose at (0,0)--and velocity distribution computed from exact theory and the approximate theory are shown in the following figures for both cases at two angles: 0 and 5 degrees (angles referenced to the unrotated foil shape). The calculations show the approximate method is sufficiently accurate for practical use at 0 degrees. At 5 degrees, the approximation is showing enough error to be questionable from a potential standpoint. However, the error is again in the direction indicated for viscous effects.

Also shown in these figures is the velocity distribution computed with $\Delta\alpha$ adjusted to give the same lift as the exact theory. These comparisons indicate that the approximate method is sufficiently accurate for most work when the lift coefficient is known.

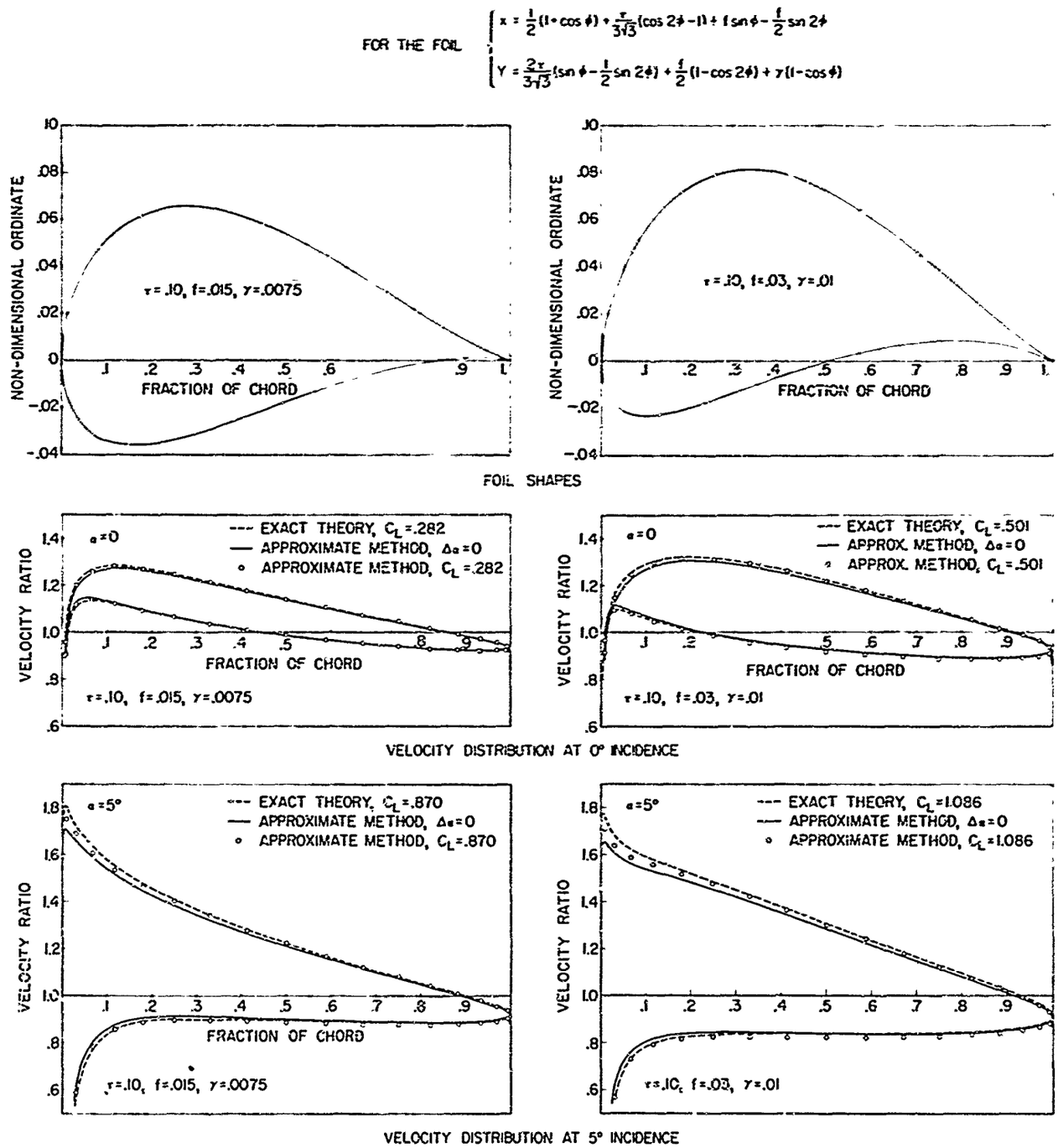

Figure A-1 — Comparison of Exact and Approximate Velocity Distribution for Foils at 0 and 5-Degree Incidence

APPENDIX B

DISCUSSION OF AIRFOIL GEOMETRY

In many cases, a thickness distribution is combined with a camberline by laying off the thickness ordinate perpendicular to the camberline.[15] One result of this combination method is a nonzero ordinate at the leading edge (the center of the nose radius lies along the camberline tangent at the leading edge[15]). A term may be added to Equation [24] to include the nonzero ordinate at the nose. However, when that was done for the NACA 4412, the computed pressure distributions gave a greater negative peak for positive incidences than either the experimental or exact potential values. This result could be anticipated from a consideration of the approximations in the theory. At the nose, the velocity due to thickness is zero and the only velocity is that of the camberline. Since the velocity at a point is considerably influenced by the ordinate at that point, a large ordinate at the nose means a large camberline velocity and correspondingly large errors in the computed velocity. To handle this nose ordinate, the profile can be rotated to put the nose at (0,0). When the pressure distribution was computed for a rotated foil, again the 4412 section, reasonable results were obtained although the predictions for potential flow ($\Delta\alpha = 0$) were somewhat lower than the exact results (see Figure 11), as expected from the comparisons in Appendix A.

In order to rotate the foil, it is first necessary to determine the nose point accurately. Points along the profile are determined from the expressions* [15]

*These expressions would follow more logically if the abscissa for the thickness ordinate were measured along the camberline. Presently, this is not done.[15]

upper surface: $(x - Y_T \sin\theta,\ Y_C + Y_T \cos\theta)$

lower surface: $(x + Y_T \sin\theta,\ Y_C - Y_T \cos\theta)$ [B-1]

where

Y_T is the thickness ordinate,

Y_C is the camberline ordinate, and

θ is the camberline inclination, $\theta = \arctan \left.\frac{dY_C}{dx}\right)_x$.

However, these expressions do not give a value for the nose point. The nose can be found by recalling that the center for the nose radius lies along the camberline tangent at the leading edge,* as below

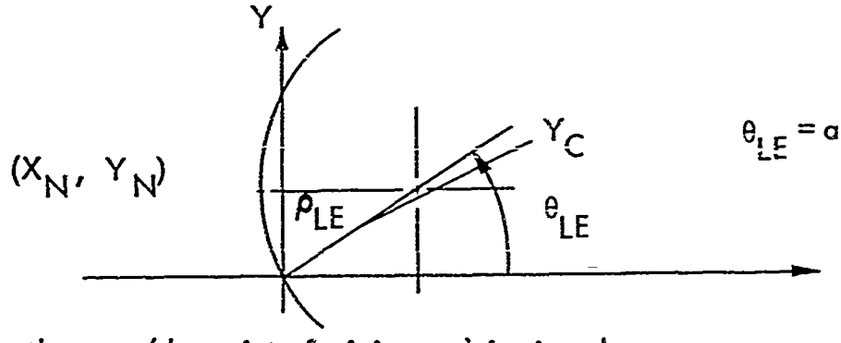

$$\theta_{LE} = \text{arc tan} \left.\frac{dY_C}{dx}\right)_{x=0}$$

Hence, the nose (the point of minimum x) is given by

$$X_N = -\rho_{LE}(1 - \cos\theta_{LE})$$

$$Y_N = \rho_{LE} \sin\theta_{LE} \qquad [B-2]$$

The nose can be put at (0,0) by the coordinate system translation (maintaining a chord length of unity):

*See footnote on preceding page.

$$X = \frac{x - X_N}{1 - X_N}$$

$$Y = \frac{Y - Y_N}{1 - X_N} \qquad [B\text{-}3]$$

Then the coordinates can be rotated through the angle

$$\omega = \arctan \frac{Y_N}{1 - X_N} \qquad [B\text{-}4]$$

to measure the ordinates from the nose-tail line. The new coordinates with a chordlength of unity are

$$X_R = \frac{X \cos \omega - Y \sin \omega}{\sqrt{1 + \left(\frac{Y_N}{1 - X_N}\right)^2}}$$

$$Y_R = \frac{Y \cos \omega + X \sin \omega}{\sqrt{1 + \left(\frac{Y_N}{1 - X_N}\right)^2}} \qquad [B\text{-}5]$$

In the pressure program, the rotated ordinates are found from Equation [B-5].

Although the above expressions are exact, they do require interpolation between the computed values, or an iteration, to find the ordinates for a fixed station. An alternative is an approximate equation for combining a camberline and thickness distribution for fixed x. Such an expression may be obtained by expanding the difference between the known ordinate in Equation [B-1] and the unknown ordinate

at x in a Taylor series. The results, retaining only the lowest order terms, are

$$Y_U = Y_C + Y_T \left[\sqrt{1 + Y_C'^2} + Y_T' Y_C'\right]$$

$$Y_L = Y_C - Y_T \left[\sqrt{1 + Y_C'^2} - Y_T' Y_C'\right] \qquad [B-6]$$

where primes denote differentiation with respect to x.

With $Y_T = 2\sqrt{\rho_{LE} x} + \ldots$ these expressions give the nose as $(0, Y_N)$ where $Y_N = \rho_{LE} Y_C'(0)$.

The rotation to put the nose at (0,0) is approximately

$$X_R \approx x$$

$$Y_R \approx Y - Y_N (1 - x) \qquad [B-7]$$

These expressions are quite accurate for small thickness and camber ratios. However, they are not used in the pressure program and are included only to show a method of combining a thickness distribution perpendicular to a camberline at fixed x so that ordinates may be obtained at the stations required in the pressure program. As already mentioned, there is a considerable saving of machine time when the ordinates are given at the required stations.

APPENDIX C

LISTING OF THE FORTRAN STATEMENTS FOR THE PRESSURE PROGRAM

```
C      ARBITRARY AIRFOIL PRESSURE DISTRIBUTION WITH MODIFICATION
C                    T. BROCKETT,DTMB CODE 5268,3/65
C
      DIMENSION X(37),Y(53),COL(17),COT(17),SY(37),VL(37),Z1(12,17),
     1   CC(53),DD(37),EE(53),ALFA(24),SO(37),CO(37),Z2(12,17),
     2    CLE(24),XA(12),SNT(12),CNT(12),ANTRP(12),Z3(12,17),
     3     Z4(12,17),D1(2,12),C1(2,12),E1(2,12)
C
C      CALCULATION OF CONSTANTS
C
      PI=3.1415927
      AN=18.0
      DO 5000 I=1,18
      TA=FLOATF(I-1)*.17453293
      CO(I)=COSF(TA)
      SO(I)=SINF(TA)
 5000 X(I)=.5*(1.+ CO(I))
      SO(19)=0.
      CO(19)=-1.
      X(19)=0.
      DO 5001 I=20,37
      IA=38-I
      X(I)=X(IA)
      CO(I)=CO(IA)
 5001 SO(I)=-SO(IA)
C
C      INTERMEDIATE  POINTS AND CORRESPONDING X VALUES
C
      DO 7777 I=1,9
 7777 ANTRP(I)=FLOATF(I)*.017453293
      ANTRP(10)=12.5*.017453293
      ANTRP(11)=15.0*.017453293
      ANTRP(12)=17.5*.017453293
      DO 4000 I=1,12
      CNT(I)=COSF(ANTRP(I))
      XA(I)=.5*(1.-CNT(I))
 4000 SNT(I)= SINF(ANTRP(I))
C
C      CALCULATION OF VECTORS USED TO OBTAIN SLOPE AND VELOCITY
C
      ERASE COL
      DO 7001 I=1,17,2
 7001 COL(I)=-1./(AN*(1.-CO(I+1)))
      COEF=1.
      DO 7002 I=1,17
      COEF=-COEF
 7002 COT(I)=COEF*SO(I+1)/(1.-CO(I+1))*.5
      DO 7003 I=1,12
      COEF=1.
      CNNT=COSF(18.*ANTRP(I))
      SNNT=SINF(18.*ANTRP(I))
      DO 7003 J=1,17
      COEF=-COEF
      TA=(-CNT(I)-CO(J+1))
      TB=(COEF*CNNT-1.)/36.
      TC= COEF*SNNT*.5
      TD=TA*TA
      TE=(1.+CO(J+1)*CNT(I))/TD
      TF=SO(J+1)*SNT(I)/TD
      TD=COEF*CNNT*.5/TA
      Z1(I,J)=TB*TF+TC*SO(J+1)/TA
      Z2(I,J)=TB*TE+TC*SNT(I)/TA
      Z3(I,J)=(TC/18.)*TF-TD*SO(J+1)
      Z4(I,J)=(TC/18.)*TE-TD*SNT(I)
 7003 CONTINUE
C
C      READ INPUT
C
 1000 READ 1,JA,KA,IPMIN
      READ 2,(ALFA(I),I=1,JA)
      READ 1,ND,IDEN,IPM,ICL
 1003 READ 3,ZA,ZB,ZC,ZD,ZE,ZF,ZG,ZH,ZI,ZJ,ZK,ZL
      IF(ICL) 100,1004,1005
 1004 READ 2,AOLE,ETA
      GO TO 1006
 1005 READ 2,(CLE(I),I=1,JA)
      ETA=0.
      AOLE=0.
 1006 IF(IPM) 100,1008,1007
 1007 READ 1,NX,ILK
      GO TO 6000
 1008 AWK=0.
      IF(IDEN) 100,101,103
  101 READ 2,(Y(I),I=1,18)
      Y(19)=0.
      ABA=Y(1)
      Y(1)=0.
      DO 102 I=1,18
      IA= 38-I
  102 Y(IA)=-Y(I)
      GO TO 104
  103 READ 2,(Y(I),I=1,36)
      Y(37)=-Y(1)
 6999 ABA=Y(1)
      Y(1)=0.
C
C      CALCULATION OF PROFILE SLOPE AND COTANGENT INTEGRAL
C
  104 IF(IDEN) 100,105,106
  105 MAD=19
      GO TO 107
  106 MAD=36
  107 DO 113 I=1,MAD
      SY(I)=0.
      VL(I)=Y(I)*9.
      DO 113 J=1,17
      LA=I-J
      IF(LA) 108,108,109
  108 LA=36+LA
  109 KB=I+J
      IF(KB-36) 112,112,110
  110 KB=KB-36
  112 SY(I)=SY(I)+(Y(LA)-Y(KB))*COT(J)
      VL(I)=VL(I)+(Y(LA)+Y(KB))*COL(J)
  113 CONTINUE
      VL(37)=VL(1)
      SY(37)=SY(1)
      IF(IDEN) 100,114,116
```

```
  114 DO 115 I=2,18
      IA=38-I
      VL(IA)=-VL(I)
  115 SY(IA)=SY(I)
  116 CONTINUE
      Y(1)=AOA
C
C     CALCULATION OF BASE PROFILE VELOCITY AND INCREMENT DUE TO ANGLE OF
C       ATTACK
C
      PRINT 25
      PRINT 6
      PRINT 37,ZA,ZB,ZC,ZD,ZE,ZF,ZG,ZH,ZI,ZJ,ZK,ZL
      PRINT 7
      DO 201 I=1,37
      D2=SQRTF(SY(I)**2+(SO(I)**2)/4.)
      CC(I)=(VL(I)-VL(I)-SO(I)/2.)/D2
      DD(I)=(SY(I)-SY(I)+(CO(I)-1.)/2.)/D2
      AAAAA=(X(I)-1.)/(2.*D2)+X(I)*DD(I)
      TA=-CC(I)
      TB=-DD(I)
      EE(I)=D2
      PRINT38,X(I),Y(I),TA,TB,AAAAA,SY(I)
  201 CONTINUE
      PRINT 9
C
C     CALCULATION OF LIFT CURVE SLOPE AND ANGLE OF ZERO LIFT,THEORY
C
      PI=(1.+2.*SY(1))**2+4.*VL(1)**2
      P=SQRTF(PI)
      AOL=ATANF(2.*VL(1)/(1.+2.*SY(1)))
      AXL=AOL*180./PI
      PRINT 5,P,AXL
      PRINT 28
C
C     CALCULATION OF BASE PROFILE VELOCITY AND INCREMENT DUE TO ANGLE OF
C     ATTACK AT INTERMEDIATE POINTS
C
      PRINT 25
      PRINT 6
      PRINT 37,ZA,ZB,ZC,ZD,ZE,ZF,ZG,ZH,ZI,ZJ,ZK,ZL
      PRINT 14
      PRINT 15
      PRINT 35
      DO 151 I=1,12
      CD1=0.
      CD2=0.
      CD3=0.
      CD4=0.
      DO 150 J=1,17
      JC=37-J
      YT=Y(J+1)-Y(JC)
      YC=Y(J+1)+Y(JC)
      CD1=CD1+YT*Z1(I,J)
      CD2=CD2+YC*Z2(I,J)
      CD3=CD3+YT*Z3(I,J)
  150 CD4=CD4+YC*Z4(I,J)
      DYU= CD3+CD4
      DYL= CD3-CD4
      CTU= CD1+CD2
      CTL=-CD1+CD2
      TA=SNT(I)*SNT(I)*.25
      TB=.5*(1.+CNT(I))
      ANTRP(I)=DYL
      E1(1,I)=SQRTF(DYU*DYU+TA)
      E1(2,I)=SQRTF(DYL*DYL+TA)
      C1(1,I)=(VL(I)-CTU-SNT(I)*.5)/E1(1,I)
      C1(2,I)=(VL(I) -CTL+SNT(I)*.5)/E1(2,I)
      D1(1,I)=(DYU-SY(I)-TB)/E1(1,I)
      D1(2,I)=(DYL-SY(I)-TB)/E1(2,I)
      AAAAA=(XA(I)-1.)/(2.*E1(1,I))+XA(I)*D1(1,5)
      TA=-C1(1,I)
      TB=-D1(1,I)
  151 PRINT36,XA(I),TA,TB,AAAAA,DYU
      PRINT 16
      PRINT 35
      DO 152 I=1,12
      AAAAA=(XA(I)-1.)/(2.*E1(2,I))+XA(I)*D1(2,I)
      TA=-C1(2,I)
      TB=-D1(2,I)
  152 PRINT36,XA(I),TA,TB,AAAAA,ANTRP(I)
      IF((CL) 100,202,503
  202 AOL=AOL+AWK
      AXL=AOL*.017453293
C
C     CALCULATION OF THEORETICAL AND DISTORTED PRESSURE DISTRIBUTION
C
  503 IF(IPMIN) 100,203,200
  200 PRINT 25
      PRINT 33
      PRINT 37,ZA,ZB,ZC,ZD,ZE,ZF,ZG,ZH,ZI,ZJ,ZK,ZL
      PRINT 34,ETA,AOLE
      PRINT 32
  203 DO 305 I=1,JA
      IF(IPMIN) 100,204,303
  204 PRINT 25
      PRINT 8
      PRINT 37,ZA,ZB,ZC,ZD,ZE,ZF,ZG,ZH,ZI,ZJ,ZK,ZL
      IF(IDEN) 100,300,301
  300 PRINT 10
      GO TO 302
  301 PRINT 11
  302 PRINT 12
  303 DMALFA=ALFA(I)+AWK
      ANG= DMALFA*.017453293
      IF(ICL) 6070,6071,6070
 6070 CL=CLE(I)
      GO TO 6072
 6071 CL=6.2831853*ETA*(ANG-AXL)
 6072 DEL=ANG-AOL-ATANF( CL/SQRTF(39.478418*PI-CL**2))
      SA=SINF(ANG)
      CA=COSF(ANG)
      IF(IPMIN) 100,6073,6074
 6073 PRINT38, DMALFA,CL,DEL,SA,ETA,AOLE
      PRINT 13
 6074 APG= ANG-DEL
      CAP=COSF(APG)
      SAP=SINF(APG)
```

```
      CLINT=0.
      CDINT=0.
      CMXINT=0.
      CMYINT=0.
      SIGMA=0.
      DO 304  J=1,37
      APG=ANG-DEL*X(J)
      CAV=COSF(APG)
      SAV=SINF(APG)
      VELP=ABSF(CC(J)*CA+DD(J)*SA)
      VELV=(1.-DEL*SO(J)/2.)*((CC(J)-VL(1)/EE(J))*CAV+(DD(J)+
     1     (.5+SY(1))/EE(J))*SAV +VL(1)/EE(J)*CAP-(.5+SY(1))/EE(J)*SAP)
      VELV=ABSF(VELV)
      ANCR=VELV-VELP
      PRESP=1.-(VELP)**2
      PRESV=1.-(VELV)**2
      ABD=PI/AN*PRESV
      ABC=ABD*SO(J)/2.
      CMXINT=CMXINT+ABC*(X(J)-.25)
      IF(IPMIN) 100,4500,4504
 4500 CDINT=CLINT-ABC
      IF(J-1) 4503,4503,4501
 4501 ABD=ABD*SY(J)
      CDINT=CDINT-ABD
      IF(J-37) 4502,4503,4503
 4502 CMYINT=CMYINT-ABD*Y(J)
 4503 CONTINUE
      PRINT38,X(J),VELP,ANCR,VELV,PRESP,PRESV
      GO TO 4506
 4504 IF(SIGMA-PRESV) 4506,4505,4505
 4505 SIGMA=PRESV
      XMIN=X(J)
      VMAX=VELV
 4506 IF(37-J) 100,4507,304
 4507 IF(IPMIN) 100,4508,4509
 4508 PRINT 17,CLINT
      PRINT 18,CDINT
      PRINT 19,CMXINT
      PRINT 20,CMYINT
C
C     CALCULATION AT INTERMEDIATE POINTS
C
      PRINT 25
      PRINT 8
      PRINT 37,ZA,ZB,ZC,ZD,ZE,ZF,ZG,ZH,ZI,ZJ,ZK,ZL
      PRINT 12
      PRINT38, DMALFA,CL,DEL,SA,ETA,AOLE
      PRINT 14
C
C     UPPER SURFACE NOSE VELOCITY
C
      PRINT 15
      PRINT 13
 4509 DO 4009 K=1,12
      APG=ANG-DEL*XA(K)
      CAV=COSF(APG)
      SAV=SINF(APG)
      VELP=ABSF(C1(1,K)*CA+D1(1,K)*SA)
      VELV=ABSF((1.-DEL*SNT(K)/2.)*((C1(1,K)-VL(1)/E1(1,K))*CAV+(D1(1,K)
     1     +(.5+SY(1))/E1(1,K))*SAV+(VL(1)*CAP-(.5+SY(1))*SAP)/E1(1,K)))
      ANCR=VELV-VELP
      PRESP=1.-(VELP)**2
      PRESV=1.-(VELV)**2
      IF(IPMIN) 100,4512,4510
 4510 IF(SIGMA-PRESV) 4009,4511,4511
 4511 SIGMA=PRESV
      XMIN=XA(K)
      VMAX=VELV
      GO TO 4009
 4512 PRINT38,XA(K),VELP,ANCR,VELV,PRESP,PRESV
 4009 CONTINUE
C
C     LOWER SURFACE NOSE VELOCITY
C
      IF(IPMIN) 100,4513,4514
 4513 PRINT 16
      PRINT 13
 4514 DO 4010 K=1,12
      APG=ANG-DEL*XA(K)
      CAV=COSF(APG)
      SAV=SINF(APG)
      VELP=ABSF(C1(2,K)*CA+D1(2,K)*SA)
      VELV=ABSF((1.+DEL*SNT(K)/2.)*((C1(2,K)-VL(1)/E1(2,K))*CAV+(D1(2,K)
     1     +(.5+SY(1))/E1(2,K))*SAV+(VL(1)*CAP-(.5+SY(1))*SAP)/E1(2,K)))
      ANCR=VELV-VELP
      PRESP=1.-VELP**2
      PRESV=1.-VELV**2
      IF(IPMIN) 100,4517,4515
 4515 IF(SIGMA-PRESV) 4010,4516,4516
 4516 SIGMA=PRESV
      XMIN=XA(K)
      VMAX=VELV
      GO TO 4010
 4517 PRINT38,XA(K),VELP,ANCR,VELV,PRESP,PRESV
 4010 CONTINUE
      IF(IPMIN) 100,305,4518
 4518 PRINT38, DMALFA,CL,SIGMA,VMAX,XMIN,CMXINT
      GO TO 305
  304 CONTINUE
  305 CONTINUE
      NO=NO-1
      IF(NO) 3000,400,1003
  400 IF(KA) 100,3000,1000
C
C     ARBITRARY INPUT SUBROUTINE
C
 6000 PRINT 25
      PRINT 21
      PRINT 37,ZA,ZB,ZC,ZD,ZE,ZF,ZG,ZH,ZI,ZJ,ZK,ZL
      IF(IDEN) 100,6150,6001
 6001 IF(ILK) 100,6020,6002
 6002 PRINT 33
      READ 2, TAU,F,RHO
      PRINT39,TAU,F,RHO
      RHO=RHO*TAU**2
      PRINT 31
      DO 6007 I=1,NX
      READ 2,AT,YT,YC,YCP
```

```
      IA=2*NX-1
      IF(AT) 100,6005,6003
 6003 IF(YCP) 6004,6006,6004
 6004 THT=ATANF(YCP*F)
      SA=SINF(THT)*YT*TAO
      CA=COSF(THT)*YT*TAO
      CC(I)=AT-SA
      Y(I)=YC*F+CA
      CC(IA)=AT+SA
      Y(IA)=YC*F-CA
      GO TO 6007
 6005 THT=ATANF(YCP*F)
      Y(I)=RHO*SINF(THT)
      YN=Y(I)
      CC(I)=-RHO*(1.-COSF(THT))
      XN=CC(I)
      GO TO 6007
 6006 Y(I)=YC*F+YT*TAO
      Y(IA)=YC*F-YT*TAO
      CC(I)=AT
      CC(IA)=AT
 6007 PRINT40,AT,YT,YC,YCP
      NX=2*NX-1
      GO TO 6030
 6020 READ 2,XN,YN
      PRINT 22
      DO 6021 I=1,NX
      READ 2,CC(I),Y(I)
 6021 PRINT39,CC(I),Y(I)
 6030 IMS=37
      B=1.-XN
      AWK=ATANF(YN/B)
      SA=SINF(AWK)
      CA=COSF(AWK)
      AWK=AWK*180./PI
      PRINT 25
      PRINT 23
      PRINT 37,ZA,ZB,ZC,ZD,ZE,ZF,ZG,ZH,ZI,ZJ,ZK,ZL
      PRINT 24,A=K
      PRINT 29
      DO 6032 I=1,NX
      CC(I)=(CC(I)-XN)/B
      Y(I)=(Y(I)-YN)/B
      ALTER=CC(I)
      CC(I)=(CC(I)*CA-Y(I)*SA)*CA
 6032 Y(I)=(Y(I)*CA+ALTER*SA)*CA
      ND=NX-1
      A=FLOATF((NX+1)/2)
      DO 6033 I=2,ND
      B=FLOATF(I)
      EE(I)=2.*CC(I)-1.
      IF(EE(I)) 6010,6016,6010
 6010 EE(I)=ATANF(SQRTF(ABSF(1.-EE(I)**2)) /CC(I))
      IF(B-A) 6011,6011,6013
 6011 IF(CC(I)-.5) 6012,6017,6033
 6012 EE(I)=EE(I)+PI
      GO TO 6033
 6013 IF (CC(I)-.5) 6014,6018,6015
 6014 EE(I)=PI+ABSF(EE(I))
      GO TO 6033
 6015 EE(I)=2.*PI-EE(I)
      GO TO 6033
 6016 IF(B-A) 6017,100,6018
 6017 EE(I)=PI/2.
      GO TO 6033
 6018 EE(I)=1.5*PI
 6033 CONTINUE
      EE(1)=0.
      EE(NX)=2.*PI
      DO 6034 I=1,NX
      A=EE(I)*180./PI
 6034 PRINT39,CC(I),Y(I),A
      GO TO 6060
 6150 PRINT 29
      ND=NX-1
      DO 6040 I=1,NX
 6040 READ 2,CC(I),Y(I)
      EE(1)=0.
      PRINT39,CC(1),Y(1),EE(1)
      DO 6155 I=2,ND
      EE(I)=2.*CC(I)-1.
      IF(EE(I)) 6151,6153,6151
 6151 EE(I)=ATANF(SQRTF(/BSF(1.-EE(I)**2)) /EE(I))
      IF(CC(I)-.5) 6152,6153,6154
 6152 EE(I)=EE(I)+PI
      GO TO 6154
 6153 EE(I)=PI/2.
 6154 A=EE(I)*180./PI
 6155 PRINT39,CC(I),Y(I),A
      EE(NX)=PI
      PRINT39,CC(NX),Y(NX),A
      IMS=19
      AWK=0.
 6060 I=1
      CC(1)=Y(1)
      R=0.
      Y1=Y(2)-Y(1)
      Y2=Y(3)-Y(1)
      Y3=Y(4)-Y(1)
      A=(Y1*EE(3)-Y2*EE(2))/(EE(2)*EE(3)*(EE(2)-EE(3)))
      B=(Y2*EE(4)-Y3*EE(3))/(EE(4)*EE(3)*(EE(3)-EE(4)))
      A3=(A-B)/(EE(2)-EE(4))
      A2=A-A3*(EE(2)+EE(3))
      A1=Y1/EE(2)-EE(2)*(A2+A3*EE(2))
 6170 R=R+.17453293
      I=I+1
      CC(I)=Y(1)+R*(A1+R*(A2+R*A3))
      IF(R-EE(2)) 6170,6170,6171
 6171 NP=NX-2
      Y1=Y(ND)-Y(NX)
      Y2=Y(NP)-Y(NX)
      N3=NX-3
      Y3=Y(N3)-Y(NX)
      R=0.
      X1=EE(ND)-EE(NX)
      X2=EE(NP)-EE(NX)
      X3=EE(N3)-EE(NX)
      A=(Y1*X2-Y2*X1)/(X1*X2*(X1-X2))
```

```
      B=(Y2*X3-Y3*X2)/(X3*X2*(X2-X3))
      AJ=(A-B)/(X1-X3)
      A2=A-AJ*(X1+X2)
      A1=Y1/X1-X1*(A2+AJ*X1)
      I=IMS
 6172 R=R-.17453293
      I=I-1
      CC(I)=Y(NX)+R*(A1+R*(A2+R*AJ))
      A=R+EE(NX)
      IF(A-EE(ND)) 6173,6173,6172
 6173 CONTINUE
 6850 DO 6855 I=2,IMS
      R=FLOAT(I-1)*.17453293
      DO 6854 J=2,NP
      IF(R-EE(J)) 6855,6853,6851
 6851 IF(R-EE(J+1)) 6852,6854,6854
 6852 JP=J-1
      X1=EE(J)-EE(JP)
      X2=EE(J+1)-EE(JP)
      X3=EE(J+2)-EE(JP)
      Y1=Y(J)-Y(JP)
      Y2=Y(J+1)-Y(JP)
      Y3=Y(J+2)-Y(JP)
      A=(Y1*X2-Y2*X1)/(X1*X2*(X1-X2))
      B=(Y2*X3-Y3*X2)/(X3*X2*(X2-X3))
      AJ=(A-B)/(X1-X3)
      A2=A-AJ*(X1+X2)
      A1=Y1/X1-X1*(A2+AJ*X1)
      R=R-EE(JP)
      CC(I)=Y(JP)+R*(A1+R*(A2+R*AJ))
      GO TO 6855
 6853 CC(I)=Y(J)
      GO TO 6855
 6854 CONTINUE
 6855 CONTINUE
      IF(IDEN) 100,6856,6858
 6856 DO 6857 I=1,18
      IA=38-I
 6857 CC(IA)=-CC(I)
 6858 CC(IMS)=Y(NX)
      DO 6907 I=1,19
      IA=38-I
      Y(I)=CC(I)
 6907 Y(IA)=CC(IA)
      Y(19)=0.
      GO TO 6999
  100 PRINT 4
C
C     INPUT/OUTPUT CONTROL
C
    1 FORMAT(4I4)
    2 FORMAT(6F12.6)
    3 FORMAT(12A6)
    4 FORMAT (24X,16H ERRONEOUS INPUT)
    5 FORMAT(1H0,41X,26HDCL/D(ALPHA)/2PI (THEORY)=,F10.6,/41X,22H ANGLE,
     1CL=0 (THEORY) =,F10.6,4H DEG)
    6 FORMAT(1H0,51X,17HPROFILE CONSTANTS)
    7 FORMAT(1H0,31X,1HX,11X,1HY,11X,1HC,11X,1HD,11X,1HE, 7X,7HDY/DPHI)
    8 FORMAT(1H0,49X,21HPRESSURE DISTRIBUTION)
    9 FORMAT(1H0,47X,24HNON-DIMENSIONAL VELOCITY/30X,21HV=(C*COS(ALFA)+D
     1*SIN(ALFA))*(1-/+DELTA*SQRT(X-X**2))+DELTA*E )
   10 FORMAT(1H0,50X,19HSYMMETRICAL PROFILE)
   11 FORMAT(1H0,48X,23HNON-SYMMETRICAL PROFILE)
   12 FORMAT(1H0,29X,4HALFA, 8X,2HCL,10X,5HDELTA, 5X,9HSIN(ALFA), 8X,10H
     1LIFT SLOPE, 3X,9HALFA,CL=0)
   13 FORMAT(1H0,31X,1HX, 6X,11HPOTNL VELOC, 1X,10HVISC INCRN, 2X,10HVIS
     1C VELOC, 3X,9HPOTNL P/Q, 3X,8HVISC P/Q)
   14 FORMAT(1H0,50X,19HINTERMEDIATE VALUES)
   15 FORMAT(1H0,53X,13HUPPER SURFACE)
   16 FORMAT(1H0,53X,13HLOWER SURFACE)
   17 FORMAT(1H0,47X,14HINTEGRATED CN=,F10.6)
   18 FORMAT(47X,15H INTEGRATED CC=,F10.6)
   19 FORMAT(39X,18H INTEGRATED CM(X)=,F10.6,13H CW ABT X=.25)
   20 FORMAT(39X,18H INTEGRATED CM(Y)=,F10.6,11H CW ABT Y=0)
   21 FORMAT(1H0,45X,27HINPUT AT ARBITRARY X VALUES)
   22 FORMAT(1H0,48X,1HX,11X,1HY)
   23 FORMAT(1H0,47X,24HROTATED AND SHRUNK INPUT)
   24 FORMAT(1H0,45X,18HANGLE OF ROTATION=,F9.6,4H DEG/33X,53HNOTE.THIS
     1ANGLE WILL BE ADDED TO EACH OF INPUT ANGLES/38X,46HTO MEASURE INCI
     2DENCE FROM INPUT REFERENCE LINE)
   25 FORMAT(1H1,30X,59HAML PROBLEM 840-041,ARBITRARY AIRFOIL PRESSURE D
     1ISTRIBUTION/41X,39HWITH EMPIRICAL CORRECTION FOR VISCOSITY)
   26 FORMAT(1H0,41X,36HNOTE,YC ORDINATE NOT USED INTERNALLY)
   29 FORMAT(1H0,48X,1HX,11X,1HY, 8X,7HPHI,DEG)
   30 FORMAT(1H0,45X,9HTHICKNESS, 5X,6HCAMBER,3X,11HNOSE RADIUS)
   31 FORMAT(1H0,43X,1HX,10X,2HYT,10X,2HYC, 8X,6HDYC/DX)
   32 FORMAT(1H0,28X,4HALFA,8X,2HCL,9X,5HCP MIN,6X,9HMAX VELOC,7X,1HX,6X
     1, 9HCM(X=.25))
   33 FORMAT(1H0,50X,17HMINIMUM PRESSURES)
   34 FORMAT(/1H0,41X,4HETA=,F8.6, 9X,11HALFA(CL=0)=,F10.6)
   35 FORMAT(1H0,36X,1HX,11X,1HC,11X,1HD,11X,1HE,     8X,7HDY/DPHI
   36 FORMAT(30X,5F12.6)
   37 FORMAT(1H0,24X,12A6)
   38 FORMAT (24X,6F12.6)
   39 FORMAT(42X,3F12.6)
   40 FORMAT(36X,4F12.6)
 3000 CALL END JOB
      END
```

REFERENCES

1. Preston, J.H., "The Calculation of Lift Taking Account of the Boundary Layer," Aeronautical Research Council R&M 2725 (1949).

2. Spence, D.A., "Prediction of the Characteristics of Two-Dimensional Airfoils," Journal of the Aeronautical Sciences, Vol. 21 (1954), p. 577.

3. Brebner, G.G. and Bagley, J.A., "Pressure and Boundary Layer Measurements on a Two-Dimensional Wing at Low Speed," Aeronautical Research Council R&M 2886 (1952).

4. Pinkerton, R.M., "Calculated and Measured Pressure Distributions over the Mid-span Section of the NACA 4412 Airfoil," National Advisory Committee for Aeronautics Report 563 (1936).

5. Betz, A., "Untersuchungen einer Schukowskyschen Tragfläche," ZFM VI, (1915), p. 173.

6. Theodorsen, T., "Theory of Wing Sections of Arbitrary Shape," National Advisory Committee for Aeronautics Report 411 (1932).

7. Riegels, F., "Uber Die Berechnung Der Druckverteilung von Profilen," Technische Brichte, Vol. 10 (1943).

8. Moriya, T., "A Method of Calculating Aerodynamic Characteristics of an Arbitrary Wing Section," Journal of the Society of Aeronautical Science, Japan, Vol. 5, No. 33 (1938), p. 7.

9. Hecker, R., "Manual for Preparing and Interpreting Data of Propeller Problems which are Programmed for the High-Speed Computers at the David Taylor Model Basin," David Taylor Model Basin Report 1244 (1959).

10. Moriya, T., "On the Aerodynamic Theory of an Arbitrary Wing Section," Journal of the Society of Aeronautical Science, Japan, Vol. 8, No. 78 (1941), p. 1054, also published in "Selected Scientific and Technical Papers," the Moriya Memorial Committee, Department of Aeronautics, University of Tokyo (Aug 1959) 1.

11. Hildebrand, F.B., "Introduction to Numerical Analysis," McGraw-Hill 1956.

12. Sokolnikoff, I.S. and Redheffer, R.M., "Mathematics of Physics and Modern Engineering," McGraw-Hill (1958).

13. Weber, J., "The Calculation of the Pressure Distribution over the Surface of Two-Dimensional and Swept Wings with Symmetrical Aerofoil Sections," Aeronautical Research Council R&M 2918 (1953).

14. Weber, J., "The Calculation of the Pressure Distribution on the Surface of Thick Cambered Wings and the Design of Wings with Given Pressure Distribution," Aeronautical Research Council R&M 3026 (1955).

15. Abbott, I.H. and von Doenhoff, A.E., "Theory of Wing Sections," Dover Publications (1959).

16. Riegels, F., "Aerofoil Sections," Butterworths, London (1961).

17. Riegels, F. and Wittich, H., "Zur Berechnung der Druckverteilung von Profilen," Jahrbuch 1942 der dtsch. Luftfahrtg., I, p. 120.

18. Hess, J.L. and Smith, A.M.O., "Calculation of the Non-Lifting Potential Flow about Arbitrary Three-Dimensional Bodies," Douglas Aircraft Co. Report ES-40622 (1962).

19. Abbott, I.H. et al., "Summary of Airfoil Data," National Advisory Committee for Aeronautics Report 824 (1945).

20. Pinkerton, R.M., "The Variation with Reynolds Number of Pressure Distribution over an Airfoil Section," National Advisory Committee for Aeronautics Report 613 (1937).

21. Kermeen, R.W., "Water Tunnel Tests of NACA 4412 and Walchner Profile 7 Hydrofoils in Noncavitating and Cavitating Flows," California Institute of Technology, Hydrodynamics Laboratory Report 47-5 (1956).

22. Kruppa, C., "Methodical Cavitation Tests of Blade Sections," Vosper Limited Report 115, Portsmouth (1963).

23. Eisenberg, P., "On the Mechanism and Prevention of Cavitation," David Taylor Model Basin Report 712 (1950); see also the addendum to this report, David Taylor Model Basin Report 842 (1953).

24. Breslin, J.P. and Landweber, L., "A Manual for Calculation of Inception of Cavitation on Two and Three-Dimensional Forms," Society of Naval Architects and Marine Engineers Technical and Research Bulletin 1-21 (Oct 1961).

25. Parkin, Blain R., "Scale Effects in Cavitating Flow," California Institute of Technology, Hydrodynamics Laboratory Report 21-8 (1952).